

1 **Wave spectral shapes in the coastal waters based on measured data off Karwar, west coast of**
2 **India**

3 Anjali Nair M, Sanil Kumar V

4 Ocean Engineering Division

5 Council of Scientific & Industrial Research-National Institute of Oceanography

6 Dona Paula 403 004, Goa India

7

8 *Correspondence to email:sanil@nio.org Tel: 0091 832 2450 327

9

10

11

12

Abstract

13

14 Understanding of the wave spectral shapes is of primary importance for the design of
15 marine facilities. In this paper, the wave spectra collected from January 2011 to December 2015 in
16 the coastal waters of the eastern Arabian Sea using the moored directional waverider buoy are
17 examined to know the temporal variations in the wave spectral shape. Over an annual cycle, for ~~For~~
18 31.15% of the time, peak frequency is between 0.08 and 0.10 Hz and the significant wave height is
19 also relatively high (~ 1.55 m) for waves in this class. The slope of the high-frequency tail of the
20 monthly average wave spectra is high during the Indian summer monsoon period (June-September)
21 compared to other months and it increases with increase in significant wave height. There is not
22 much interannual variation in slope for swell dominated spectra during the monsoon, while in the
23 non-monsoon period, when wind-seas have much influence, the slope varies significantly. Since the
24 exponent of the high-frequency partslope of the wave spectrum is within the range from -4 to -3-4
25 during the monsoon period, Donelan spectrum shows better fit for the high-frequency part of the
26 wave spectra in monsoon months compared to other months.

27

28 **Key Words:** Ocean surface waves, wind waves, Arabian Sea, wave spectrum, high-frequency tail

29

30 1. Introduction

31

32 Information on wave spectral shapes are required for designing ~~the~~ marine structures
33 (Chakrabarti, 2005) and almost all the wave parameters computations are based on the wave
34 spectral function (Yuan and Huang, 2012). The growth of waves and the correspondent spectral
35 shape is due to the complex ocean-atmosphere interactions, while the physics of air-sea interaction
36 is not completely understood (Cavaleri et al., 2012). The shape of the wave spectrum depends on
37 the factors governing the wave growth and decay, and a number of spectral shapes have been~~are~~
38 proposed in the past for different sea states (see Chakrabarti, 2005 for a review). The spectral
39 shape is maintained by nonlinear transfer of energy through nonlinear four-wave interactions
40 (quadruplet interactions) and white-capping (Gunson and Symonds, 2014). The momentum flux
41 between the ocean and atmosphere govern the high-frequency wave components (Cavaleri et al.,
42 2012). According to Philips, the equilibrium ranges for low-frequency and high-frequency region is
43 proportional to f^5 and f^4 (where f is the frequency) respectively. Several field studies made since
44 JONSWAP (Joint North Sea Wave Project) field campaign reveals~~reveal~~ an analytical form for
45 wave spectra with the spectral tail proportional to f^4 (Toba, 1973; Kawai et al., 1977; Kahma,
46 1981; Forristall, 1981; Donelan et al., 1985). Usually, there is a predominance of swell fields in
47 large oceanic areas, which is due to remote storms (Chen et al., 2002; Hwang et al., 2011; Semedo
48 et al., 2011). The exponent used in the expression for the frequency tail has different values (see
49 Siadatmousavi et al., 2012 for a brief review). For shallow water, Kitaigordskii et al. (1975)
50 suggested f^{-3} tail, Liu (1989) suggested f^{-4} for growing young wind-seas and f^{-3} for fully developed
51 wave spectra. Badulin et al. (2007) suggested f^4 for frequencies where nonlinear interactions are
52 dominant. The study carried out at Lake George by Young and Babanin (2006) revealed that in the
53 frequency range $5f_p < f < 10f_p$, the average value of the exponent 'n' of f^{-n} is close to 4. Whereas,
54 some studies in real sea conditions indicate that high-frequency shape of f^4 -applies up to few times
55 the peak frequency (f_p) and then decays faster with frequency. The spectra for coastlines in
56 Currituck Sound with short fetch condition showed a decay closer to f^5 when f is greater than two
57 or three times the peak frequency (Long and Resio, 2007). Gagnaire-Renou et al. (2010) found- that
58 the energy input from wind and dissipation due to white-capping have a significant influence on the
59 high-frequency tail of the spectrum.

60

Formatted: Tab stops: 2.5 cm, Left + 4.99 cm, Left + 5.49 cm, Left + 6 cm, Left + 6.99 cm, Left + 7.99 cm, Left + 8.99 cm, Left + 9.99 cm, Left + 10.99 cm, Left + 11.99 cm, Left

61 The physical processes in the north Indian Ocean have a distinct seasonal cycle (Shetye et
62 al., ~~1985; Ranjha et al., 2015~~) and the surface wind-wave field is no exception (Sanil Kumar
63 et al., 2012). In the eastern ~~Arabian Sea (AS)~~, significant wave height (H_{m0}) up to 6 m is
64 measured in the monsoon period (June to September), and during rest of the period, H_{m0} is
65 normally less than 1.5 m (Sanil Kumar and Anand, 2004). Sanil Kumar et al. (2014) observed that
66 in the eastern AS, the wave spectral shapes are different at two locations within 350 km distance,
67 even though the difference in the integrated parameter like H_{m0} is marginal. Dora and Sanil Kumar
68 (2015) observed that waves at 7-m water depth in the nearshore zone off Karwar are high energy
69 waves in the monsoon and low to moderate waves in the non-monsoon period (January to May and
70 October to December). Dora and Sanil Kumar (2015) study shows similar contribution of wind-
71 seas and swells during the pre-monsoon (February to May), while swells dominate the wind-sea in
72 the post-monsoon (October to January) and the monsoon period. A study was carried out by Glejin
73 et al. (2012) to find the variation in wave characteristics along the eastern AS and the influence of
74 swells in the nearshore waves at 3 locations during the monsoon period in 2010. This study shows
75 that the percentage of swells in the measured waves was 75 to 79% at the locations with higher
76 percentage of swells in the northern portion of AS compared to that at the southern side. Wind and
77 wave data measured at a few locations along the west coast of India for short-period, one to two
78 months as well as the wave model results were analysed to study the wave characteristics in the
79 deep as well as nearshore regions during different seasons (Vethamony et al., 2013). From the wave
80 data collected for two years period (2011 and 2012) along the eastern AS, the swells of period more
81 than 18 s and significant wave height less than 1 m which occur for 1.4 to 3.6% of the time were
82 separated and their characteristics were studied by Glejin et al. (Earlier, 2016). Anjali Nair and Sanil
83 Kumar (2016) presented the daily, monthly, seasonal and annual variations in the wave spectral
84 characteristics for a location in the eastern AS and reported that over an annual cycle, 29 % of the
85 wave spectra are single-peaked spectra and 71 % are multi-peaked spectra. Recently Amrutha et al.
86 (2017) by analysing the measured wave data in October reported that the high waves (significant
87 wave height > 4 m) generated in an area bounded by 40-60° S and 20-40° E in the south Indian
88 Ocean reached the eastern AS in 5-6 days and resulted in the long-period waves. The earlier studies
89 indicate that the spectral tail of the high-frequency part shows large variation and its variation with
90 seasons are not known. Similarly, the shape of the parametric spectra are also different and hence it
91 is important to identify the spectral shapes based on the measured data covering all the seasons and
92 different years.

Formatted: English (United States)

93

94 The ~~previous~~ discussion above shows that there is a strong inspiration to study the high-
95 frequency tail of the wave spectrum. For the present study, we used the directional waverider buoy
96 measured wave spectral data at 15-m water depth off Karwar, west coast of India, over 5 years
97 during 2011 to 2015 and evaluated the nearshore wave spectral shapes in different months. This
98 study addresses two main questions: (1) How the high-frequency tail of the wave spectrum varies in
99 different months, and? (2) What are the spectral parameters for the best-fit theoretical spectra, ?
100 This paper is organized as follows: the study area is introduced in section 2, details of data used and
101 methodology in section 3. Section 4 presents the results of the study and the conclusions are given
102 in section 5.

103

104 2. Study area

105

106 The coastline at Karwar is 24° inclined to the west from the north, and the 20 m depth
107 contour is inclined 29° to the west. Hence, large waves in the nearshore will have an incoming
108 direction close to 241°, since waves get aligned with the depth contour due to refraction. At 10, 30
109 and 75 km distance from Karwar, the depth contours of 20, 50 and 100 m are present (Fig. 1). The
110 study region is under the seasonally reversing monsoon winds, with winds from the northeast
111 during the post-monsoon and from the southwest during the monsoon period. The monsoon winds
112 are strong and the total seasonal rainfall is 280 cm. The average monthly sea level at Karwar varies
113 from 1.06 m (in September) to 1.3 m (in January) with respect to chart datum and the average tidal
114 range is 1.58 m during spring tides and 0.72 m during neap tides (Sanil Kumar et al., 2012).

115

116 3. ~~Data~~Materials and methods

117

118 The waves off Karwar (14° 49' 56" N and 74° 6' 4" E) ~~were~~ measured using the
119 directional waverider buoy (DWR-MKIII) (Barstow and Kollstad, 1991). Measurements are carried
120 out from 1 January 2011 to 31 December 2015. The data of heave and two translational motion of
121 for every 30 minutes from the buoy are sampled continuous records at 3.84 Hz. A digital high-pass
122 filter with a cut off at 30 s is applied to the 3.84 Hz samples. At the same time it converts the
123 sampling rate to 1.28 Hz and stores the time series data at 1.28 Hz, ~~are processed as one record.~~
124 From the time series data for 200s, the wave spectrum is obtained through a fast Fourier transform

125 (FFT). During half an hour 8 wave spectra of a 200 s data interval each are collected and averaged
126 to get a representative wave spectrum for half an hour (Datawell, 2009). The wave spectrum is with
127 a resolution of 0.005 Hz from 0.025 Hz to 0.1 Hz and is 0.01 Hz from 0.1 to 0.58 Hz. Bulk wave
128 parameters; significant wave height (H_{m0}) which equals $4\sqrt{m_0}$ and mean wave period (T_{m02}) based
129 on second order moment, which equals $\sqrt{m_0/m_2}$ are obtained from the spectral moments. Where
130 m_n is the n^{th} order spectral moment ($m_n = \int_0^\infty f^n S(f) df$, $n=0$ and 2), $S(f)$ is the spectral energy
131 density and ~~f is the~~ frequency. The spectral peak period (T_p) is estimated from the wave
132 spectrum and the peak wave direction (D_p) is estimated based on circular moments (Kuik et al.,
133 1988). The wind-seas and swells are separated through the method described by Portilla et al.
134 (2009) and the wind-sea and the swell parameters are computed by integrating over the respective
135 spectral parts. Measurements reported here are in Coordinated Universal Time (UTC), which is
136 05:30 h behind the local time. U_{10} is the wind speed at 10-m height obtained from reanalysis data of
137 zonal and meridional components at 6 hourly intervals from NCEP / NCAR (Kalnay et.al., 1996)
138 and is used to study the influence of wind speed on the spectral shape.-

139
140 Since the frequency bins over which the wave spectrum estimated is same in all years, the
141 monthly and seasonally averaged wave spectrum is computed by taking the average of the spectral
142 energy density at the respective frequencies of each spectrum over the specified time.

143
144 Wave spectrum continues to develop through non-linear wave-wave interactions even for
145 very long times and distances. Hence, most of the wave spectrum is not fully developed and cannot
146 be represented by Pierson-Moskowitz (PM) spectrum (Pierson and Moskowitz, 1964). Accordingly,
147 an additional factor was added to the PM spectrum in order to improve the fit to the measured
148 spectrum. The JONSWAP spectrum (Hasselmann et al., 1973) is thus a PM spectrum multiplied by
149 an extra peak enhancement factor γ . The high-frequency tail of the JONSWAP spectrum decays in
150 a form proportional to f^{-5} . A number of studies reported that high-frequency decay is by a form
151 proportional to f^{-4} . Modified JONSWAP spectrum including Toba's formulation of saturation range
152 was proposed by Donelan et al. (1985). The JONSWAP and Donelan spectrum used in the study
153 are given in eqns. (1) and (2).

154
$$S(f) = \frac{\alpha g^2}{(2\pi)^4 f^5} \exp \left[-\frac{5}{4} \left(\frac{f}{f_p} \right)^{-4} \right] \gamma \exp \left[-\frac{(f-f_p)^2}{2\sigma^2 f_p} \right] \dots\dots\dots (1)$$

155
$$S(f) = \frac{\alpha g^2}{(2\pi)^4 f^4 f_p} \exp \left[-\left(\frac{f}{f_p} \right)^{-4} \right] \gamma \exp \left[-\frac{(f-f_p)^2}{2\sigma^2 f_p^2} \right] \dots\dots\dots (2)$$

156 Where γ is the peak enhancement parameter; α is Philip's constant; f is the wave frequency; g is the
 157 gravitational acceleration -and σ is the width parameter.

158
$$\sigma = \begin{cases} 0.07, & f < f_p \\ 0.09, & f \geq f_p \end{cases}$$

159 An exponential curve $y = k.f^b$ is fitted for high-frequency part of the spectrum and the
 160 exponent (value of b) is estimated for the best fitting curve based on statistical measures such as
 161 least square error and bias. The slope of the high-frequency part of the wave spectrum is
 162 represented by the exponent of the high-frequency tail.

163 For the present study, JONSWAP spectrum is tested by fitting for the whole frequency
 164 range of the measured wave spectrum. It is found out that the JONSWAP spectra do not show a
 165 good fit for higher frequency range, whereas Donelan spectrum shows better fit for the high-
 166 frequency range. Hence, JONSWAP spectrum is used for the lower frequency range up to spectral
 167 peak and Donelan spectrum is used for the higher frequency range from the spectral peak for
 168 single-peaked wave spectrum. Theoretical wave spectra are not fitted to the double-peaked wave
 169 spectra.

170
 171
 172

173 **4. Results and discussions**

174
 175 4.1 Bulk wave parameters

176
 177 Mostly the wave conditions (~ 75%) at the buoy location are intermediate and shallow-
 178 water waves (where water depth is less than half the wavelength, $d < L/2$), this condition is not
 179 satisfied during ~ 25% of the time due to waves with mean periods of 4.4 s or less. This study.

Formatted: Font: (Default) Arial, English (India)

180 therefore, deals with shallow, intermediate and deepwater wave climatology. Hence, bathymetry
181 will significantly influence the wave characteristics.

182
183 The persistent monsoon winds generate choppy seas with average wave heights of 2 m and
184 mean wave period of 6.5 s. Fig. 2 shows that in~~the~~ the monsoon, the observed waves had a
185 maximum H_{m0} of about 5 m, with H_{m0} of 2-2.5 m more common during this period. The and the
186 maximum H_{m0} measured during the study period is on 21 June 2015 17:30 UTC (Fig. 2a). Mean
187 wave periods (T_{m02}) at the measurement location ranged from 4-8 s (Fig. 2b). Wave direction
188 during monsoon is predominantly from the west due to refraction towards the coast. The fluctuation
189 in H_{m0} due to the southwest monsoon is seen in all the years (Fig. 2a). High waves ($H_{m0} > 2$ m)
190 during 27-29 November 2011 are~~is~~ due to the deep depression ARB04 formed in the AS, Arabian
191 Sea (AS). During the study period, the annual average H_{m0} is same (~1.1 m) in all the years (Table
192 1). In 2013, the data during August could not be collected and hence resulted in lower annual
193 average H_{m0} . Over the 5 years, small waves ($H_{m0} < 1$ m) account for a large proportion (63.94%) of
194 measured data and only during 0.16% of the time, H_{m0} exceeded 4 m (Table 2). The 25th and 75th
195 percentiles of the H_{m0} distribution over the entire analysis period are 0.6 and 1.4 m.

196
197 Waves with low heights—Small waves ($H_{m0} < 1$ m) are with the mean period in a large
198 range (2.7-10.5 s), whereas high waves ($H_{m0} > 3$ m) have mean wave period in a narrow range (6.1-
199 9.3 s) (Table 2). For waves with H_{m0} higher-more than 3 m, the T_p never exceeded 14.3 s and for
200 waves with H_{m0} less than 1 m, T_p up to 22.2 s are observed (Fig. 2c) and the long period swells
201 (14-20 s) are with $H_{m0} < 2.5$ m. Around 7% of the time during 2011-2015, waves have peak period
202 more than 16.7 s (Table 3). Peak frequencies~~frequency~~ between 0.08 and 0.10 Hz, equivalent to a
203 peak wave period of 10 - 12.5 s are~~is~~ observed in 31.15% of the time and the H_{m0} is also relatively
204 high (~ 1.55 m) for waves in this class. During the annual cycle, the wave climate is dominated by
205 low waves ($0.5 > H_{m0} > 1$ m); intermediate-period ($T_p \sim 10$ -16s) south-westerly swell. Waves from
206 the northwest are with T_p less than 8 s (Fig. 3).

207
208 The wave roses during 2011-2015 indicate that around 38% of the time during the period
209 2011 to 2015, the predominant wave direction is SSW (225°) with long period (14 - 18s) and
210 intermediate period (10 - 14s) waves (Fig. 3). A small percentage of long-period waves having H_{m0}
211 more than 1m are observed from the same direction in which more than 80% are swells (Fig. 3c).

Formatted: English (United States)

Formatted: (Complex) Arabic (Saudi Arabia), English (India)

Formatted: Line spacing: 1.5 lines

212 Intermediate period waves observed having H_{m0} less than 1m, contain 20 - 60% of swells. Around
213 10-15% of the waves observed during the period are from the west, which includes intermediate
214 and short period waves with H_{m0} varying from 1.5 to 3m. These intermediate period waves from
215 west having H_{m0} between 2.5 - 3m contain more than 80% of swells. Waves from NW are short
216 period waves with H_{m0} between 0.5 and 1.5; in which swell percentage is very less showing the
217 influence of wind-sea ~~generated by sea breeze~~ (Fig. 3d). High waves observed in the study area
218 consists of more than 80% swells.

219
220 Date versus year plots of significant wave height (Fig. 4) shows that H_{m0} has its maximum
221 values ($H_{m0} > 3m$) during the monsoon period with a wave direction of WSW and peak wave period
222 of 10 - 12s (intermediate period). The mean wave period shows its maximum values (6 - 8s) during
223 the monsoon period. During January–May in all the years, H_{m0} is low ($H_{m0} < 1m$) with waves from
224 SW, W and NW directions. NW waves observed are the result of strong sea breezes existing during
225 this period. Both long-period ($T_p > 14s$), intermediate-period ($10 < T_p < 14s$) and short-period (T_p
226 $< 8s$) waves are observed during this period and hence, the mean wave period observed is low
227 compared to the monsoon (Fig. 4d). During October to December, similar to the pre-monsoon
228 period, H_{m0} observed is less than 1m, but the wave direction is predominantly from SW and W, with
229 least NW waves. Short period waves are almost absent during this period, and the condition is
230 similarsame for all the years. The interannual variations in H_{m0} are less than 15% (Fig. 4). Primary
231 seasonal variability in waves is due to the monsoonal wind reversal. During January-March, there is
232 a shift ~~in~~ the occurrences of northwest swells.

233
234 ~~Most~~ 4.2 Wave spectrum
235
236 ~~of the wave conditions (~75%) are to be intermediate and shallow water waves at the buoy~~
237 ~~location (where water depth is less than half the wavelength, $d < L/2$), this condition is not satisfied~~
238 ~~during ~25% of time due to waves with mean periods of 4.4 s or less. This study, therefore, deals~~
239 ~~with shallow, intermediate and deepwater wave climatology. Hence, bathymetry will significantly~~
240 ~~influence the wave characteristics.~~

241
242 Normalisation of the wave spectrum is done to know the spread of energy in different
243 frequencies. Since the range of maximum spectral energy density in a year is large (~ 60 m²/Hz),
244 each wave spectrum is normalised through dividing the spectral energy density by the maximum
245 spectral energy density of that spectrum. 4.2 Wave spectrum

Formatted: English (United States)

Formatted: (Complex) Arabic (Saudi Arabia), English (India)

Formatted: Line spacing: 1.5 lines

246
247 | ———The normalized wave spectral energy density contours are presented for different years to
248 know the wind-sea/swell predominance (Fig. 5). The predominance of both the wind-seas and
249 swells are observed in the non-monsoon period, whereas in the monsoon only swells are
250 predominant (Fig. 5). The separation of swells and wind-seas indicates that over~~Over~~ an annual
251 cycle, around 54% of the waves are ~~due to~~-swells. Glejin et al. (2012) reported that the dominance
252 of swells during monsoon is due to the fact that even though the wind at the study region is strong
253 during monsoon, the wind over the entire AS also will be strong and when these swells are added to
254 the wave system at the buoy location, the energy of the ~~-swell~~ increases (Donelan, 1987) and will
255 result in dominance of swells. The spread of spectral energy to higher frequencies (0.15 to 0.25 Hz)
256 is predominant during January-May (Fig. 5) due to sea-breeze in the pre-monsoon period (Neetu et
257 al., 2006; Dora and Sanil Kumar, 2015). In the monsoon during the wave growth period, the
258 spectral peak ~~shifts~~~~shifted~~ from 0.12-0.13 Hz to 0.07-0.09 Hz (lower frequencies).

260 | ———An interesting phenomenon is that the long-period (> 18 s) swells are present for
261 2.5% of the time during the study period. The buoy location at 15 m water depth is exposed to
262 waves from northwest to south with the nearest landmass at ~ 1500 km in the northwest (Asia), \sim
263 2500 km in the west (Africa), ~ 4000 km in the southwest (Africa) and ~ 9000 km in the south
264 (Antarctica) (Amrutha et al., ~~2016~~2017). Due to its exposure to the Southern Oceans and the large
265 fetch available, swells are present all year round in the study area and the swells are dominant in the
266 non-monsoon (Glejin et al., 2013). Throughout the year, waves with period more than 10 s (the
267 low-frequency (< 0.1 Hz) waves) are the southwest swells whereas with seasons the direction of
268 short-period~~high frequency~~ waves changes (Fig. 5). Amrutha et al. (2017)~~(2016)~~ reported that the
269 long-period waves observed in the eastern AS are the swells generated in the south Indian Ocean.
270 In the monsoon season, the waves with high-frequency are predominantly from west-southwest,
271 whereas in the non-monsoon they are from the northwest. In the non-monsoon period, the
272 predominance of wind-seas and swells fluctuated and hence the mean wave direction also changed
273 frequently (Fig. 5). The average direction of waves with $H_{m0} < 1$ m shows the northwest wind-seas
274 and the southwest swells, whereas, for high waves ($H_{m0} > 3$ m), the difference between the swell
275 and wind-sea direction decreases. This is because the high waves get aligned to the bottom contour
276 before 15 m water depth on its approach to the shallow water.

Formatted: Indent: First line: 1.27 cm

Formatted: English (United States)

Formatted: English (United States)

Formatted: (Complex) Arabic (Saudi Arabia), English (United Kingdom)

278 The interannual changes of wave spectral energy density for different months in the period
279 2011-2015 are studied by computing the monthly average wave spectra for all the years (Fig. 6).
280 ~~In~~Except during the non-monsoon period, the wave spectra observed is double-peaked, indicating
281 the presence of wind-seas and swells, whereas during the monsoon, due to the strong southwest
282 winds, single peaked spectrum is observed, i.e. the swell peak with low-frequency and high spectral
283 energy density. Along the Indian coast, Harish and Baba (1986), Rao and Baba (1996) and Sanil
284 Kumar et al. (2003) found out that ~~wave the~~ spectra are generally multi-peaked and ~~that~~ the double
285 peaked wave spectra are more frequent during low-sea states (Sanil Kumar et al., 2004). Sanil
286 Kumar et al. (2014), Sanil Kumar and Anjali (2015) and Anjali and Sanil Kumar (2016) have also
287 observed ~~that~~ double-peaked spectrum in the monsoon period in the eastern AS are due to the
288 locally generated wind-seas and the south Indian Ocean swells. ~~In the study area, from~~ From
289 January to May and October to December, the swell peak is between the frequencies 0.07 and 0.08
290 Hz ($12.5 < T_p < 14.3s$), ~~14.28s~~); but in the monsoon period, the swell peak is around 0.10 Hz, in all
291 the years studied. This shows long-period swells ($T_p > 13s$) in the non-monsoon period and
292 intermediate period swells ($8 < T_p < 13s$) in the monsoon. Glejin et al. (2016), also observed the
293 presence of low-amplitude long-period waves in the eastern AS in the non-monsoon period and
294 intermediate period waves in the monsoon period. This is because of the propagation of swells from
295 the southern hemisphere is more visible during the non-monsoon period due to the calm conditions
296 (low wind-seas) prevailing in the eastern AS. Whereas during the monsoon period, these swells are
297 less due to the turbulence in the north Indian Ocean (Glejin et al., 2013). Large interannual
298 variations are observed for monthly average wave spectrum in all months except in July. This is
299 because July is known to be the roughest month over the entire annual cycle and southwest
300 monsoon reaches its peak during July. Hence, the influence of temporally varying wind-seas on the
301 wave spectrum is least during July compared to other months. ~~Due~~Maximum spectral energy
302 ~~observed is during June 2013 due~~ to the early onset (on 1 June) and advancement of monsoon
303 during 2013 compared to other ~~years, the monthly average value of the maximum spectral energy is~~
304 ~~observed in June 2013 (Fig. 6).~~ years. The wave spectra of November 2011 is distinct from that of
305 other years, with low wind-sea peak frequency, i.e. 0.13 Hz due to the deep depression ARB04,
306 occurred south of India near Cape Comorin, during 26 November–1 December, with a sustained
307 wind speed of 55 km/h. During October 2014, the second peak is observed at 0.11 Hz with
308 comparatively high energy showing the influence of cyclonic storm NILOFAR. It is an extremely
309 severe cyclonic storm ~~that~~ occurred during the period 25-31 October 2014, originated from a low-

310 pressure area between Indian and Arabian Peninsula, with the highest wind speed of 215 km/h and
311 affected the areas of India, Pakistan and Oman. Significant interannual variation is observed in the
312 wind-sea peak frequency. Wave spectra averaged over each season (Fig. 7) shows that the
313 interannual variations in energy spectra averaged over full year period almost follows the pattern of
314 wave spectra averaged over monsoon period spectra, indicating the strong influence of monsoon
315 winds over the wave energy spectra in the study area. Interannual variations within the spectrum
316 are more for wind-sea regions compared to swell regions. During the study period, the maximum
317 spectral energy observed is during 2011 monsoon.

318
319 For different frequencies, the monthly average wave direction is shown in -Fig. 8. It is
320 observed that throughout the year the mean wave direction of the swell peak is southwest (200-
321 250°). In the non-monsoon period, the wind-sea direction is northwest (280-300°), except in
322 October and November. This is due to the wind-seas produced by sea breeze which has the
323 maximum intensity during the pre-monsoon season. Interannual variability in wave direction is
324 highest during October and November, where the wind-seas from southwest direction are also
325 observed. This is because, during these months, the wind speed and the strength of the monsoon
326 swell decreases, which makes the low energy wind-seas produced by the withdrawing monsoon
327 winds more visible.

328
329 Contour plots of spectral energy density (normalized) clearly show the predominance of
330 wind-seas and swells during the non-monsoon period (Fig. 9). In the monsoon period, the spectral
331 energy density is mainly confined to a narrow frequency range (0.07-0.14 Hz) and the wave spectra
332 are mainly single peaked with maximum energy within the frequency range 0.08-0.10 Hz, having
333 direction 240°. Glejin et al. (2012) reported that in the monsoon season, the spectral peak is
334 between 0.08 and 0.10 Hz (12-10s) for ~ 72% of the time in the eastern AS. Earlier studies also
335 reported dominance of swells in the eastern AS during the monsoon (Sanil Kumar et al., 2012;
336 Glejin et al., 2012). Above 0.15 Hz, energy gradually decreases, with the lowest energy observed
337 between 0.30 and 0.50 Hz. Wind-sea energy is comparatively low during October, November and
338 December and occurs mostly in the frequency range less than 0.20 Hz, whereas, during January-
339 May, the frequency exceeds 0.20 Hz. In the pre-monsoon period, wind-sea plays a major role in
340 nearshore wave environment (Rao and Baba, 1996). Wind-sea energy is found to be low during

341 April 2015 (Fig. 6), because of reduction in local winds. The occurrence of wind-seas is very less
342 during most of the time in November except during 2011, due to the deep depression ARB04.

343
344 ~~To study the characteristics of different wave systems, average mean wave direction and~~
345 ~~average wave spectral energy density grouped under different peak frequency bins are plotted in~~
346 ~~Fig. 10. Wave spectrum is mostly single peaked at low frequency bins and multi peaked at higher~~
347 ~~frequencies. Within the frequency range 0.07 to 0.15 Hz, the spectrum observed is a smooth single~~
348 ~~peaked spectrum, with high energy density. Maximum energy observed is within the frequency~~
349 ~~range 0.08-0.1 Hz, having direction 240° which indicates the monsoon swells. Above 0.15 Hz, even~~
350 ~~though the spectrum is multi peaked, energy gradually decreases, with the lowest energy observed~~
351 ~~between 0.3 and 0.5 Hz. Between 0.15 and 0.5 Hz, waves observed are from the northwest~~
352 ~~direction (300°) and represents the wind seas produced by local winds. Long period swells ($T_p >$~~
353 ~~14s) are also observed from the southwest. The average direction of waves with $H_{m0} < 1\text{m}$ shows~~
354 ~~the northwest wind seas and the southwest swells, whereas for high waves ($H_{m0} > 3\text{m}$), the~~
355 ~~difference between the swell and wind sea direction decreases (Fig. 11). This is because the high~~
356 ~~waves get aligned to the bottom contour before 15 m water depth on its approach to the shallow~~
357 ~~water.~~

358
359 The behavior of the high-frequency part of the spectrum is governed by the energy balance
360 of waves generated by the local wind fields. When the wind blows over a long fetch or for a long
361 time, the wave energy for a given frequency reaches the equilibrium range and the energy input
362 from the wind ~~isare~~ balanced by energy loss to ~~lowerother~~ frequencies and by wave breaking
363 (Torsethaugen and Haver, 2004). The high-frequency tail slope of the monthly average wave
364 spectrum in different years (~~Table 4~~) shows that the slope is high (~~b < -~~(~~→~~3.1), during June to
365 September and the case is same for all the years studied (~~Table 4~~). During all other months, the
366 ~~exponent in the expression for the frequency tail slope~~ is within the range ~~1.5- 3.1 to -1.5~~. The
367 distribution of ~~exponentslope~~ values for different significant wave height ranges shows that the
368 slope increases (~~exponent decrease~~ from ~~-2.44 to -4.20~~) as the significant wave height increases
369 and reaches a saturation range. For frequencies from ~~0.230-229~~ to 0.58 Hz in the eastern AS during
370 January-May, Amrutha et al. (2017)(2016) observed that the high-frequency tail has $f^{2.5}$ pattern at
371 15 m water depth and for frequencies ranging from 0.315 to 0.55 Hz, the high-frequency tail
372 follows f^3 at 5 m water depth. ~~It is shown in Fig. 12 that the slope also increases as the mean wave~~

373 ~~period increases.~~ Since H_{m0} is maximum during the monsoon period, the slope is also maximum
374 during June to September. There is no much interannual variation in slope for swell dominated
375 spectra during the monsoon, while in the non-monsoon period when wind-seas have much
376 influence, the slope varies significantly. ~~The slope of the high-frequency end of the wave spectrum
377 becomes milder when the wave nonlinearity increases. The study shows that the tail of the
378 spectrum is influenced by the local wind conditions.~~

Formatted: Font color: Red,
(Complex) Hindi (India), English (India)

379 380 ~~4.3 Theoretical wave spectra~~

Formatted: Default

381
382 ~~———— The monthly average wave spectra for the year 2015, is compared with JONSWAP
383 and Donelan theoretical wave spectra. It is found that JONSWAP and Donelan spectra with
384 modified parameters describe well the wave spectra at low frequencies and high frequencies
385 respectively.~~ The most obvious manifestations of nonlinearity are sharpening of the wave crests and
386 the flattening of the wave troughs and these effects are reflected in the skewness of the sea surface
387 elevation (Toffoli, 2006). Zero skewness indicates linear sea states, positive skewness value
388 indicate that the wave crests are bigger than the troughs. Figure 10 shows that nonlinearity
389 increases with increase in H_{m0} . The slope of the high-frequency end of the wave spectrum becomes
390 steeper when the wave nonlinearity increases. Donelan et al. (2012) find that in addition to the k^{-4}
391 dissipation that swells modulate the equilibrium in breaking waves dependent on the mean surface
392 slope, while Melville (1994) also quantified a relation between wave packet slopes and dissipation
393 rate. These results are specific to breaking waves, but one might expect similar relations between
394 surface dynamics and dissipation rate for non breaking waves. A function of the form: $A * \exp(\lambda$
395 $H_{m0}) + s0$, with initial parameters of $A = 8$, $\lambda = -2.4$, $s0 = -3.7$ is found to fit the exponent of the
396 high-frequency tail data with the significant wave height (Fig. 11a). The functional representation
397 of the exponent of the high-frequency tail data with H_{m0} shown in Fig. 11a might be useful in
398 revealing the physical connection, and at the very least would provide a predictive basis relating
399 spectral slopes with mean significant wave heights as a basis for future research. It is shown in Fig.
400 11b that the exponent decreases (slope increases) as the mean wave period increases. The study
401 shows that the tail of the spectrum is influenced by the local wind conditions (Fig. 11c) and the
402 influence is more with the zonal component (u) of the wind than on the meridional component (v)
403 (Figs. 11e and 11f). The exponent of the high-frequency tail decreases with the increase of the
404 inverse wave age (U_{10}/c), where c is the celerity of the wave.

405
406
407
408
409
410
411
412
413
414
415
416
417
418
419
420
421
422
423
424
425
426
427
428
429
430
431
432
433
434
435
436

4.3 Comparison with theoretical wave spectra

~~From Fig. 13, we can see that spectrum is double peaked during January April and December. For these months the first peak is fitted with JONSWAP spectrum and second with Donelan, and the fitted spectrum shows a good match with the measured one.~~ In the monsoon period, the spectrum is single peaked with high spectral energy density and during this period JONSWAP spectrum is fitted up to the peak frequency and after that Donelan spectrum is used. The monthly average wave spectra during the monsoon period for the year 2011, is compared with JONSWAP and Donelan theoretical wave spectra in Figure 12. ~~During the months May, October and November, after the peak frequency, the measured spectrum is not smooth and hence for this part, Donelan spectrum is fitted in two parts in order to obtain the best fit. Here also JONSWAP shows best fit, up to the peak frequency.~~

It is found that JONSWAP and Donelan spectra with modified parameters describe well the wave spectra at low frequencies and high frequencies respectively. The values for α and γ were randomly varied within a range to find out the values for which, the theoretical spectrum best fits the measured spectrum and those values were used to plot the theoretical spectrum. The values of α and γ thus obtained, for June, July, August each month and September the range of frequencies for which each spectrum is plotted are given in Table 6. From the table, the average values of α and γ , for the monsoon months over 1 year period are obtained as 0.00090.0050 and 1.821.33 for JONSWAP spectra and 0.02740.0254 and 1.641.27 for Donelan spectra respectively. These values are less than the generally recommended values of α and γ ; 0.0081 and 3.3. α is a constant that is related to the wind speed and fetch length. For all the data, Donelan spectrum fitted is proportional to f^n , where n is the exponent value of the high-frequency tail. ~~From the table, it can be seen that α has the highest values during the months June to August and is the same for both JONSWAP and Donelan spectrum. This may be due to the high wind speed during monsoon. High values of α were also observed during November, February and April, since these are the months during which sea breeze has maximum influence, high α values is due to the influence of local winds. There is no seasonal variation observed in the values of γ . For all the months, Donelan spectrum fitted is proportional to f^4 , except during May and November, where spectrum is proportional to $f^{2.8}$ and $f^{2.5}$, above frequencies 0.15 Hz and 0.28 Hz respectively.~~ The theoretical spectrum JONSWAP and

Formatted: Indent: First line: 0 cm

437 Donelan cannot completely describe the high-frequency tail of the measured spectrum since the
438 high-frequency tail in these spectrum decays in the form of f^{-5} and f^{-4} respectively. Since the
439 exponent of the high-frequency tail slope of the wave spectrum is within the range 3-4 to -3 during
440 the monsoon period, Donelan spectrum shows better fit for monsoon spectra compared to other
441 months (Fig. 11,13).

442

443 5. Concluding remarks

444

445 In this paper, the variations in the wave spectral shapes in different months for a nearshore
446 location are investigated, based on in situ wave data obtained from a moored directional waverider
447 buoy. Interannual variations within the spectrum are more for wind-seas compared to swells. The
448 maximum significant wave height measured at 15 m water depth is 5 m and the annual average H_{m0}
449 has similar value (~ 1.1 m) in all the years. Over the 5 years, small waves ($H_{m0} < 1$ m) account for a
450 large proportion of measured data (63.94% of the time). The study shows that high waves ($H_{m0} > 2$
451 m) are with spectral peak period between 8 and 14 s and the long period swells (14-20 s) are with
452 $H_{m0} < 2.5$ m. The high-frequency slope of the wave spectrum (the exponent decreases/ varies from -
453 2.44 to -4.20) and it increases with increase in significant wave height and mean wave period.
454 During the monsoon period, Donelan spectrum shows better fit for monsoon spectra compared to
455 other months since the exponent of the high-frequency part slope of the wave spectrum is within the
456 range 3-4 to -3. The decay of the high-frequency waves are fastest with depth and hence, the high-
457 frequency tail values observed in the study will be different for different water depths.

458

459 Acknowledgments

460 The authors acknowledge the Earth System Science Organization, Ministry of Earth
461 Sciences, New Delhi for providing the financial support to conduct part of this research. We thank
462 TM Balakrishnan Nair, Head OSISG and Arun Nherakkol, Scientist, INCOIS, Hyderabad and Jai
463 Singh, Technical Assistant, CSIR-NIO for the help during the collection of data. We thank Dr. Bhat
464 and Dr. J L Rathod, Department of Marine Biology, Karnataka University PG Centre, Karwar for
465 providing the logistics required for wave data collection. This work contributes part of the Ph.D.
466 work of the first author. This paper is dedicated to the memory of our esteemed colleague Ashok
467 Kumar, in recognition of his substantial contributions in initiating the long-term wave
468 measurements in the shallow waters around India. We thank the topic editor and both the reviewers

469 for their critical comments and the suggestions which improved the scientific content of the
470 publication. This publication is a NIO contribution.

471
472 **References**
473

474 Amrutha, M.M., Sanil Kumar, V., and George, J.: ObservationsCharacteristics of inter monsoon
475 long-period waves in the nearshore waters of central west coast of India during the fall inter-
476 monsoon period, Ocean Engineering, 131, 244-262, 10.1016/j.oceaneng.2017.01.014, 2017. (in
477 review), 2016.

Formatted: els-display-text

Formatted: els-display-text

478 Anjali, N.M., and Sanil Kumar, V.: Spectral wave climatology off Ratnagiri - northeast Arabian
479 Sea, Natural Hazards, 82, 1565-1588, 2016.

480 Badulin, S.I., Babanin, A.V., Zakharov, V.E. and Resio, D.: Weakly turbulent laws of wind-wave
481 growth, Journal of Fluid Mechanics., 591, 339-378, 2007.

482 Ardhuin, F., Chapron, B., and Collard, F.: Observation of swell dissipation across oceans, J.
483 Geophys. Res. Oceans., 36, 1-5, 2009.

484 Carter, R.W.G.: Coastal environments: an introduction to the physical, ecological and cultural
485 systems of coastlines, in: Academic Press., London, 1988.

486 Cavaleri, L., Fox-Kemper, B., and Hemer, M.: Wind-waves in the coupled climate sys- tem. Bull.
487 Am. Meteorol. Soc., 93, 1651-1661, 2012.

488 Chakrabarti, S.K.: Handbook of Offshore Engineering, Vol-1, Ocean Engineering Series, Elsevier,
489 p 661, 2005.

490 Chen, G., Chapron, B., Ezraty, R., and Vandemark, D.: A global view of swell and wind-sea
491 climate in the ocean by satellite altimeter and scatterometer. J. Atmospheric and Oceanic
492 Technology., 19(11), 1849-1859, 2002.

493 Datawell.: Datawell Waverider Reference Manual. Datawell BV oceanographic instruments, The
494 Netherlands, Oct. 10, pp.123, 2009.

495 ~~Chen, Q., Zhao, H., Hu, K., and Douglass, S.L.: Prediction of Wind Waves in a Shallow Estuary, J.~~
496 ~~Waterway, Port, Coastal, and Ocean Eng., 131 (4), 137-148, 2005.~~

497 ~~Dattatri, J.: Coastal Erosion and Protection along Karnataka Coast, Centre for Environmental Law,~~
498 ~~Education, Research and Advocacy (CEERA), The National Law School of India University, 2007.~~

499 Donelan, M. A.: The effect of swell on the growth of wind waves, Johns Hopkins APL Technical
500 Digest., 8 (1), 18-23, 1987.

501 Donelan, M., Hamilton, H., and Hui, W.H.: Directional spectra of wind-generated waves,
502 Philosophical Transactions of the Royal Society of London A: Mathematical, Physical and
503 Engineering Sciences., 315(1534), 509-562, 1985.

504 ~~Donelan, M.A., Curcic, M., Chen, S.S. and Magnusson, A.K.: Modeling waves and wind stress,~~
505 ~~Journal of Geophysical Research: Oceans., 117(C11), 2012.~~

506 Dora, G.U., and Sanil Kumar, V.: Sea state observation in island-sheltered nearshore zone based on
507 in situ intermediate-water wave measurements and NCEP/CFSR wind data, Ocean Dynamics., 65,
508 647-663, 2015.

509 ~~Forristall, G.Z.: Measurements of a saturated range in ocean wave spectra, Journal of Geophysical~~
510 ~~Research: Oceans., 86(C9), 8075-8084, 1981. Gagnaire-Renou, E., Benoit, M. and Forget, P.: Ocean~~
511 ~~wave spectrum properties as derived from quasi-exact computations of nonlinear wave-wave~~
512 ~~interactions, Journal of Geophysical Research: Oceans., 115(C12), 2010.~~

513 ~~Drennan, W. M., Kahma, K.K., and Donelan, M.A.: On momentum flux and velocity spectra over~~
514 ~~waves, Boundary Layer Meteorology., 92(3), 489-515, 1999.~~

515 Glejin, J., Sanil Kumar, V., Balakrishnan Nair, T. M., and Singh, J.: Influence of winds on
516 temporally varying short and long period gravity waves in the near shore regions of the eastern
517 Arabian Sea, Ocean Sci., 9, 343–353, doi:10.5194/os-9-343-2013, 2013.

518 Glejin, J., Sanil Kumar, V., Sajiv, P.C., Singh, J., Pednekar, P., Ashok Kumar, K., Dora, G.U., and
519 Gowthaman, R.: Variations in swells along eastern Arabian Sea during the summer monsoon, Open
520 J. Mar. Sci., 2 (2), 43–50, 2012.

521 | Glejin, J., Sanil Kumar, V., Amrutha, M.M. and Singh J.: Characteristics of long-period swells
522 | measured in the in the near shore regions of eastern Arabian Sea, Int. J. Naval Architecture and
523 | Ocean Engineering, 8, 312-319, 2016.

524 | ~~Goda, Y.: A review on statistical interpretation of wave data, Report of the Port and Harbour
525 | Research Institute, Japan 18, 5-32, 1979.~~

526 | ~~Goda, Y.: On the methodology of selecting design wave height, Proceedings 21st International
527 | Conference Coastal Engineering, Malaga, 899-913, 1988.~~

528 | ~~Gringorten, I.I.: A plotting rule for extreme probability paper, J. Geophysical Res., 68 (3), 813-814,
529 | 1963.~~

530 | ~~Guedes Soares, C., Cherneva, Z., and Antao, E.M.: Steepness and asymmetry of the largest waves
531 | in storm sea states, Ocean Eng., 31(8), 1147-1167, 2004.~~

532 | ~~Gumbel, E.J.: Statistics of Extremes, Columbia University Press, New York, USA, 1958.~~

533 | Gunson, J., and Symonds, G.: Spectral Evolution of Nearshore Wave Energy during a Sea-Breeze
534 | Cycle, J. Phys. Oceanogr., 44(12), 3195-3208, 2014.

535 | ~~Hanamgond, P.T., and Mitra, D.: Dynamics of the Karwar Coast, India, with special reference to
536 | study of Tectonics and Coastal Evolution using Remote Sensing Data, J. Coastal Research., Special
537 | Issue 50, 842-847, 2007.~~

538 | ~~Hanley, K. E., Belcher, S.E., and Sullivan, P.P.: A global climatology of wind-wave interaction, J.
539 | Phys. Oceanogr., 40(6), 1263-1282, 2010.~~

540 | ~~Hanson, J.L., and Phillips, O.M.: Wind-sea growth and dissipation in the open ocean, J. Phys.
541 | Oceanogr., 29, 1633-1648, 1999.~~

542 | Harish, C. M., and Baba, M.: On spectral and statistical characteristics of shallow water waves,
543 | Ocean Eng., 13(3), 239-248, 1986.

544 | Hasselmann, K., Barnett, T.P., Bouws, F., Carlson, H., Cartwright, D.E., Enke, K., Ewing J.A.,
545 | Gienapp, H., Hasselmann, D.E., Krusemann, P., Meerburg, A., Muller, P., Olbers, D.J., Richter, K.,

546 Sell, W., and Walden, H.: Measurements of wind-wave growth and swell decay during the Joint
547 North Sea Wave Project (JONSWAP), Deutsches Hydrographisches Institut., A8 (12), 95, 1973.

548 ~~Hasselmann, K., Ross, D.B., Miller, P., and Sell, W.: A parametric wave prediction model, J. Phys.~~
549 ~~Oceanogr., 6, 200-228, 1976.~~

550 ~~Houlihujsen, L. H.: Waves in oceanic and coastal waters, Cambridge University Press, 2007.~~

551 Hwang, P.A., Garcia-Nava, H., and Ocampo-Torres, F.J.: Dimensionally Consistent Similarity
552 Relation of Ocean Surface Friction Coefficient in Mixed Seas, J. Phys. Oceanogr 41., 1227–1238.
553 2011.

554 Kahma, K.K.: A study of the growth of the wave spectrum with fetch, Journal of Physical
555 Oceanography., 11(11), 1503-1515, 1981.

556 Kalnay, E., Kanamitsu, M., Kistler, R., Collins, W., Deaven, D., Gandin, L., Iredell, M., Saha, S.,
557 White, G., Woollen, J. and Zhu, Y.: The NCEP/NCAR 40-year reanalysis project. Bulletin of the
558 American meteorological Society., 77(3), 437-471, 1996.

559 Kawai, S., Okada, K. and Toba, Y.: Field data support of three-seconds power law and σ^{-4} -
560 spectral form for growing wind waves, Journal of Oceanography., 33(3), 137-150, 1977.

561 Kitaigor'skii, S.A., Krasitskii, V.P. and Zaslavskii, M.M.: On Phillips' theory of equilibrium range
562 in the spectra of wind-generated gravity waves, Journal of Physical Oceanography., 5(3), 410-420,
563 1975.

564 Kuik, A. J., Vledder, G., and Holthuijsen, L.H.: A method for the routine analysis of pitch and roll
565 buoy wave data, J. Phys. Oceanogr., 18, 1020–1034, 1988.

566 Liu, A.K., Jackson, F.C., Walsh, E.J. and Peng, C.Y.: A case study of wave-current interaction near
567 an oceanic front, Journal of Geophysical Research: Oceans., 94(C11), 16189-16200, 1989.

568 Long, C.E. and Resio, D.T.: Wind wave spectral observations in currituck sound, north Carolina,
569 Journal of Geophysical Research: Oceans., 112(C5), 2007.

570 Longuet-Higgins, M.S.: On the joint distribution of the periods and amplitudes of sea waves, J.
571 Geophys. Res.-Oceans., 80, 2688–2694, 1975.

572 Neetu, S., Shetye Satish., and Chandramohan, P.: Impact of sea breeze on wind-seas off Goa, west
573 coast of India, Journal Earth System Science., 115, 229-234, 2006.

574 ~~Nigam, R., and Khare, N.: Significance of correspondence between river discharge and proloculus~~
575 ~~size of benthic Foraminifera in paleomonsoonal studies, Geo Marine Letters., 15 (1), 45-50, 1995.~~

576 Pierson, W.J., and Moskowitz, L.: A proposed form for fully developed seas based on the similarity
577 theory of S.A. Kitaigorodski, J. Geophys. Res.-Oceans., 69(24), 5181-5190, 1964.

578 Portilla, J., Ocampo-Torres, F.J., and Monbaliu, J.: Spectral Partitioning and Identification of
579 Wind-sea and Swell, J. Atmospheric and Oceanic Technology., 26, 117-122, 2009.

580 Ranjha, R., Tjernström, M., Semedo, A., Svensson, G.: Structure and variability of the Oman
581 Coastal Low-Level Jet, Tellus A, 67, 25285, <http://dx.doi.org/10.3402/tellusa.v67.2528> , 2015.

582 Rao, C. P., and Baba, M.: Observed wave characteristics during growth and decay: a case study,
583 Continental Shelf Res., 16(12), 1509-1520, 1996.

584 Sanilkumar, V., Ashokkumar, K. and Raju, N.S.N.: Wave characteristics off Visakhapatnam coast
585 during a cyclone, Indian Academy of Sciences., 2004.

586 Sanil Kumar, V., Johnson, G., Dora, G.U., Chempalayil, S.P., Singh, J., and Pednekar, P.:
587 Variations in nearshore waves along Karnataka, west coast of India, J. Earth Systems Science., 121,
588 393-403, 2012.

589 Sanil Kumar, V., Anand, N.M., Kumar, K.A., and Mandal, S.: Multipeakedness and groupiness of
590 shallow water waves along Indian coast, J. Coastal Res., 19, 1052-1065, 2003.

591 Sanil Kumar, V., and Anand, N.M.: Variation in wave direction estimated using first and second
592 order Fourier coefficients, Ocean Eng., 31, 2105–2119, 2004.

593 Sanil Kumar, V. and Anjali Nair, M.: Inter-annual variations in wave spectral characteristics at a
594 location off the central west coast of India, Ann. Geophys., 33, 159–167, doi:10.5194/angeo-33-
595 159-2015, 2015.

596 ~~Sanil Kumar, V., and Kumar, K.A.: Spectral representation of high shallow water waves, Ocean~~
597 ~~Eng., 35, 900-911, 2008.~~

598 | ~~Sanil Kumar, V.,~~Shanas, P.R., and Dubhashi, K.K.: Shallow water wave spectral characteristics
599 | along the eastern Arabian Sea, *Natural Hazards*, 70, 377–394, 2014.

600 | Semedo, A., Sušelj, K., Rutgersson, A., and Sterl, A.: A global view on the wind-sea and swell
601 | climate and variability from ERA-40, *J. Climate*, 24(5), 1461-1479, 2011.

602 | Shetye, S.R., Shenoi, S.S.C., Antony, A.K., and Kumar, V.K.: Monthly-mean wind stress along the
603 | coast of the north Indian Ocean, *J. Earth Syst. Sci.*, 94, 129–137, doi:10.1007/BF02871945, 1985.

604 | Shore Protection Manual., U.S. Army Coastal Engineering Research Center, Department of the
605 | Army, Corps of Engineers, U.S. Govt. Printing Office, Washington, DC, USA, vols. 1 and 2, 1984.

606 | Siadatmousavi, S.M., Jose, F. and Stone, G.W.: On the importance of high frequency tail in third
607 | generation wave models, *Coastal Engineering.*, 60, 248-260, 2012.

608 | Toba, Y.: Local balance in the air-sea boundary processes, *Journal of Oceanography.*, 29(5), 209-
609 | 220, 1973.

610 | Toffoli, A., Onorato, M. and Monbaliu, J.: Wave statistics in unimodal and bimodal seas from a
611 | second-order model, *European Journal of Mechanics B/Fluids*, 25, 649–661, 2006.

612 | ~~Stephen, F.B., and Tor Kollstad.: Field trials of the directional waverider, *Proceedings of the First*~~
613 | ~~*International Offshore and Polar Engineering Conference, Edinburgh, III 55–63, 1991.*~~

614 | Torsethaugen, K., and Haver, S.: Simplified double peak spectral model for ocean waves, In:
615 | *Proceeding of the 14th International Offshore and Polar Engineering Conference*, 2004.

616 | Vethamony, P., Rashmi, R., Samiksha, S.V. and Aboobacker, M.: Recent Studies on Wind Seas
617 | and Swells in the Indian Ocean: A Review, *International J. Ocean and Climate Systems*, 4, 63 - 73,
618 | 2013.

619 | Young, I.R. and Babanin, A.V.: Spectral distribution of energy dissipation of wind-generated
620 | waves due to dominant wave breaking, *Journal of Physical Oceanography.*, 36(3), 376-394, 2006.

621 | Yuan, Y., and Huang, N.E.: A reappraisal of ocean wave studies, *J. Geophys. Res.-Oceans.*,
622 | 117(C11), 2012.

623 |

Formatted: Don't adjust space between Latin and Asian text, Don't adjust space between Asian text and numbers, Tab stops: 2.5 cm, Left + 4.99 cm, Left + 5.49 cm, Left + 6 cm, Left + 6.99 cm, Left + 7.99 cm, Left + 8.99 cm, Left + 9.99 cm, Left + 10.99 cm, Left + 11.99 cm, Left

624 **Figure captions**

625 Figure 1. Study area along with the wave measurement location in eastern Arabian Sea

626 Figure 2. Time series plot of a) significant wave height, b) mean wave period, c) peak wave period
627 and d) mean wave direction from 1 January 2011 to 31 December 2015. Thick blue line indicates
628 the monthly average values

629 Figure 3. Wave roses during 2011-2015 (a) significant wave height and mean wave direction, (b)
630 peak wave period and mean wave direction, (c) percentage of swell, (d) percentage of wind-sea and
631 mean wave direction

632 Figure 4. Date versus year plot of a) significant wave height b) mean wave direction, c) peak wave
633 period and d) mean wave period

634 Figure 5. Temporal variation of normalized spectral energy density (top panel) and mean wave
635 direction (bottom panel) with frequency in different years

636 Figure 6. Monthly average wave spectra in 2011 to 2015

637 Figure 7. Wave spectra averaged over a) pre-monsoon (February-May), b) monsoon (June-
638 September), c) post-monsoon (October-January) and d) full year in different years

639 Figure 8. Monthly average wave direction at different frequencies in different months

640 Figure 9. Temporal variation of normalized spectral energy density in different months (data from
641 2011 to 2015 used)

642 Figure 10. ~~Scatter plot~~Plot of ~~significant average spectral energy density and average mean~~ wave
643 ~~height with skewness~~direction of ~~the sea surface elevation in~~waves grouped under different
644 ~~years~~peak frequency bins

645 Figure 11. ~~Plot of~~ ~~exponent~~a) average spectral energy density and b) average mean wave direction
646 of ~~the waves under different H_{m0} with frequency~~

647 ~~Figure 12. Plot of~~ high-frequency tail with a) significant wave height, b) ~~(left panel) and with~~
648 ~~mean wave period, c) wind speed, d) inverse wave age, e) u-wind and f) v-wind (right panel)~~

649 ~~Figure 12.13.~~ Fitted theoretical spectra along with the monthly average wave spectra for different
650 month

651

652 Table 1. Number of data used in the study in different years along with range of significant wave
 653 height and average value
 654

Year	Significant wave height (m)		Number of data	%of data
	Range	Average		
2011	0.3-4.4	1.1	17517	99.98
2012	0.3-3.7	1.1	17323	98.61
2013	0.3-3.6	0.9*	14531	82.94
2014	0.3-4.5	1.1	17284	98.65
2015	0.3-5.0	1.1	14772	84.32

655 * average value is estimated excluding the ~~July~~August month data
 656
 657
 658
 659
 660
 661

662 Table 2. Characteristics of waves in different range of significant wave height
 663

Significant wave height range	Number (percentage)	Range of Tp (s)	Mean Tp (s)	Range of T _{m02} (s)	Mean T _{m02} (s)
$H_{m0} < 1$ m	52062 (63.94)	2.6-22.2	12.2	2.7-10.5	4.9
$1 \leq H_{m0} < 2$ m	18297 (22.47)	3.6-22.2	10.5	3.4-10.7	5.7
$2 \leq H_{m0} < 3$ m	9839 (12.08)	6.2-18.0	10.8	5.0-8.9	6.5
$3 \leq H_{m0} < 4$ m	1096 (1.35)	10.0-14.3	11.8	6.1-9.1	7.2
$4 \text{ m} \leq H_{m0}$	133 (0.16)	10.5-14.3	12.6	7.2-9.3	7.8

664
 665
 666
 667
 668
 669
 670 Table 3. Average wave parameters and number of data in different spectral peak frequencies
 671

Frequency (f_p) range (Hz)	Number of data and %	H_{m0} (m)	T _{m02} (s)	Peak wave period (s)
$0.04 < f_p \leq 0.05$	318 (0.39)	0.73	5.24	20.19
$0.05 < f_p \leq 0.06$	5341 (6.56)	0.82	5.48	17.16
$0.06 < f_p \leq 0.07$	14764 (18.13)	0.75	5.22	14.73
$0.07 < f_p \leq 0.08$	18221 (22.38)	0.80	5.05	12.96
$0.08 < f_p \leq 0.10$	25364 (31.15)	1.55	5.76	10.88
$0.10 < f_p \leq 0.15$	9459 (11.62)	1.25	5.35	8.07
$0.15 < f_p \leq 0.20$	6355 (7.80)	0.76	4.43	5.72
$0.20 < f_p \leq 0.30$	1487 (1.83)	0.78	3.86	4.36
$0.30 < f_p \leq 0.50$	118 (0.14)	0.66	3.22	3.09

672

673
 674 | Table 4. Exponent Slope of the high-frequency tail of the monthly average wave spectra in
 675 different years
 676

Months	<u>Exponent of the high-High</u> frequency tail					
	2011	2012	2013	2014	2015	2011-2015
January	-2.08	-2.93	-2.97	-2.72	-2.81	-2.72
February	-2.41	-3.02	-2.74	-2.99	-3.06	-2.85
March	-2.75	-2.91	-2.82	-2.76	No data	-2.81
April	-2.56	-2.74	-2.64	-2.71	-2.19	-2.60
May	-2.59	-2.67	-2.63	-2.42	-2.51	-2.56
June	-3.64	-3.53	-3.55	-3.82	-3.58	-3.55
July	-3.76	-3.55	<u>No data-</u> <u>3.40</u>	-3.82	-3.63	-3.70
August	-3.63	-3.58	<u>-3.40</u> <u>No data</u>	-3.52	-3.65	-3.58
September	-3.41	-3.44	-3.16	-3.38	-3.00	-3.30
October	-2.02	-2.77	-3.03	-2.52	-2.61	-2.68
November	-1.78	-2.43	-1.77	-1.55	-1.65	-1.84
December	-1.69	-2.23	-1.95	-2.06	-1.79	-1.94

677
 678
 679
 680
 681
 682
 683
 684 | Table 5. Exponent of the high-High frequency tail of the average wave spectra in different wave
 685 height ranges
 686

Range of H_{m0} (m)	<u>Exponent of the high-High</u> frequency tail <u>parameter</u>
0-1	-2.44
1-2	-3.26
2-3	-3.67
3-4	-4.21
4-5	-4.21

Formatted Table
 Formatted: Centered

689 | Table 6. Parameters of the fitted wave spectrum in different yearsmonths

690

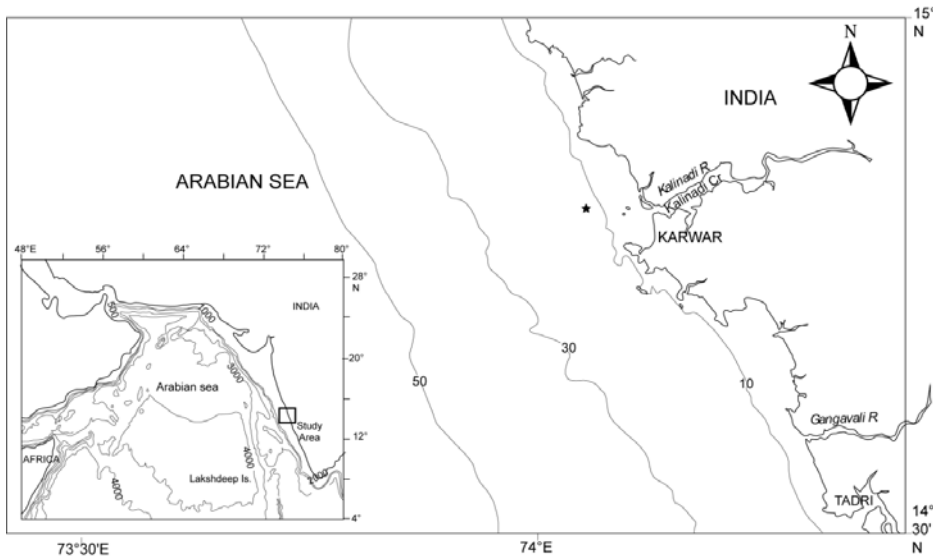
691

Year		JONSWAP spectrum		Donelan spectrum	
		α	γ	α	γ
2011	June	0.0013	2.2	0.0028	2.0
	July	0.0016	1.5	0.0021	1.7
	August	0.0013	1.8	0.0029	1.7
	September	0.0004	2.3	0.0021	1.6
2012	June	0.0015	1.6	0.0029	2.0
	July	0.0010	2.1	0.0031	1.9
	August	0.0009	2.2	0.0032	1.7
	September	0.0006	2.0	0.0024	1.8
2013	June	0.0006	3.3	0.0030	1.9
	July	No data			
	August	0.0012	1.1	0.0038	1.4
	September	0.0005	1.9	0.0042	1.4
2014	June	0.0010	1.1	0.0010	1.6
	July	0.0006	2.5	0.0019	1.2
	August	0.0006	1.5	0.0021	1.2
	September	0.0011	1.1	0.0032	1.4
2015	June	0.0011	1.4	0.0023	1.8
	July	0.0011	1.9	0.0024	1.8
	August	0.0008	1.8	0.0024	1.4
	September	0.0006	1.3	0.0043	1.6

692

693

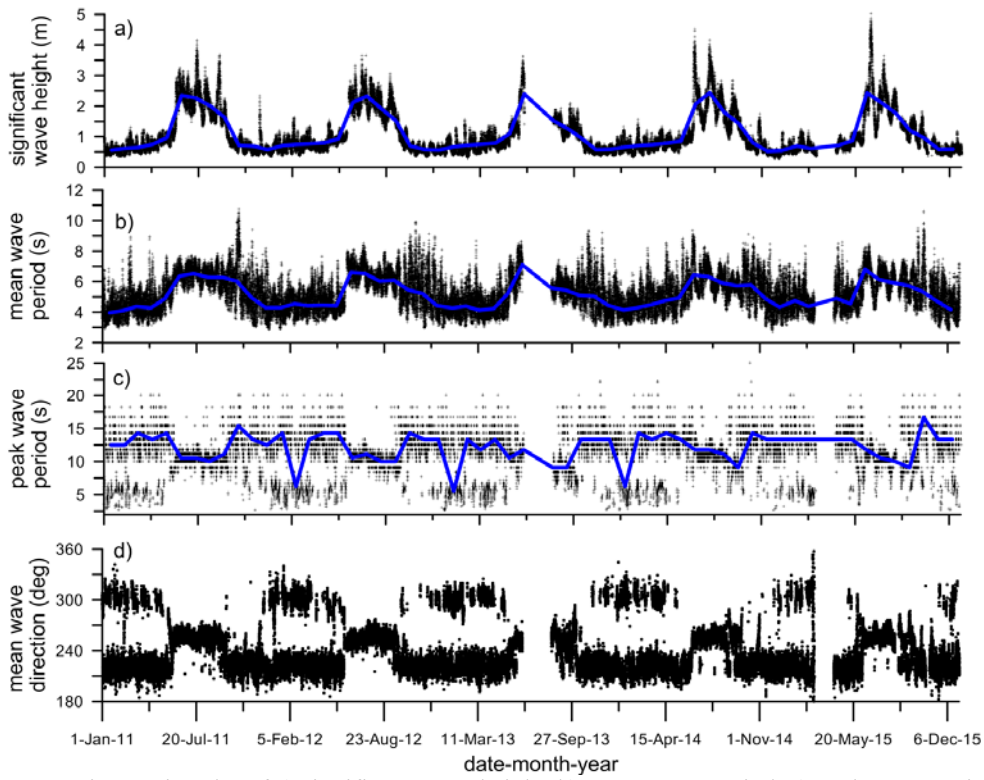
694



695

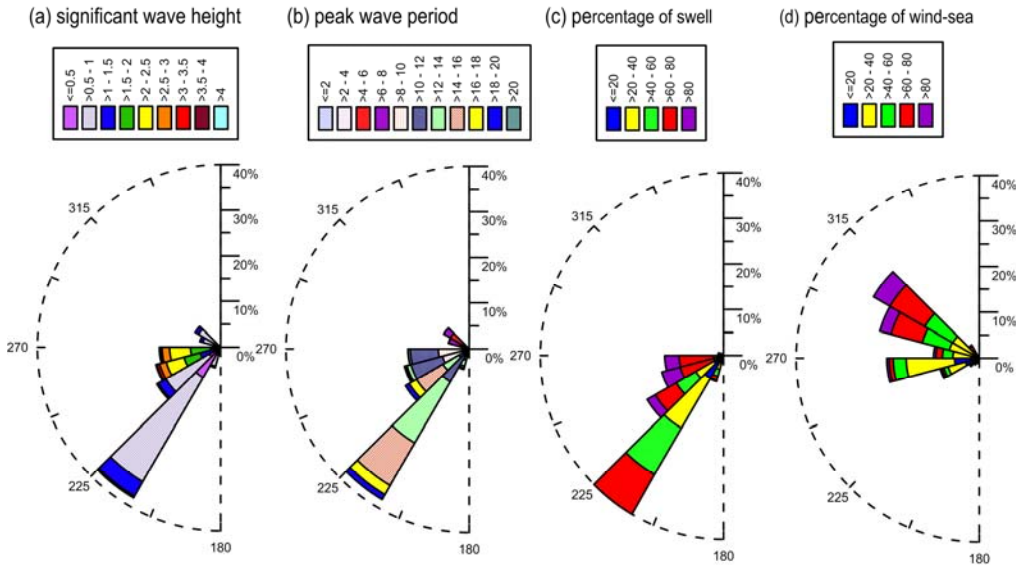
696 Figure 1. Study area along with the wave measurement location in eastern Arabian Sea
697

698
699



700
701 Figure 2. Time series plot of a) significant wave height, b) mean wave period, c) peak wave period
702 and d) mean wave direction from 1 January 2011 to 31 December 2015. Thick blue line indicates
703 the monthly average values
704 |

705



706

707

708

709

710

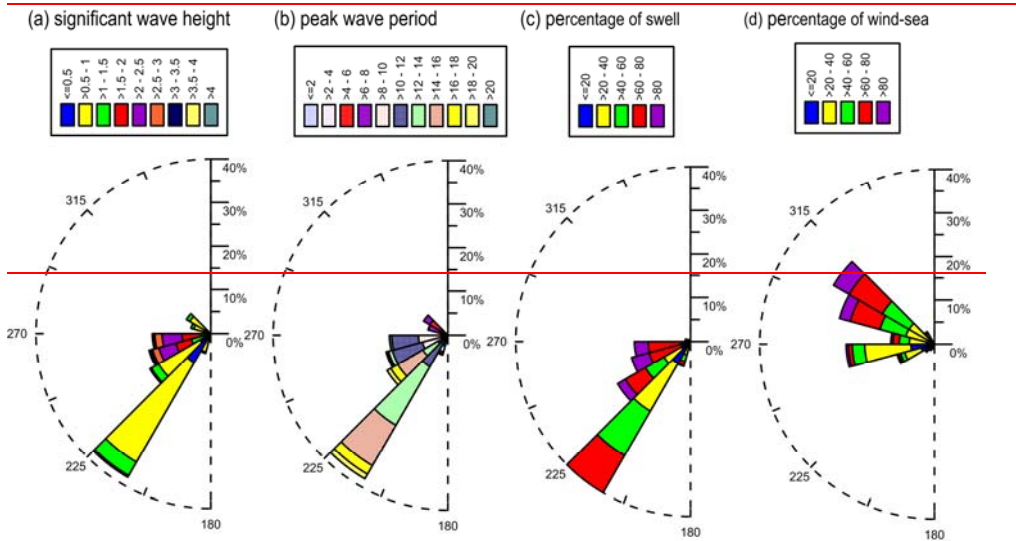
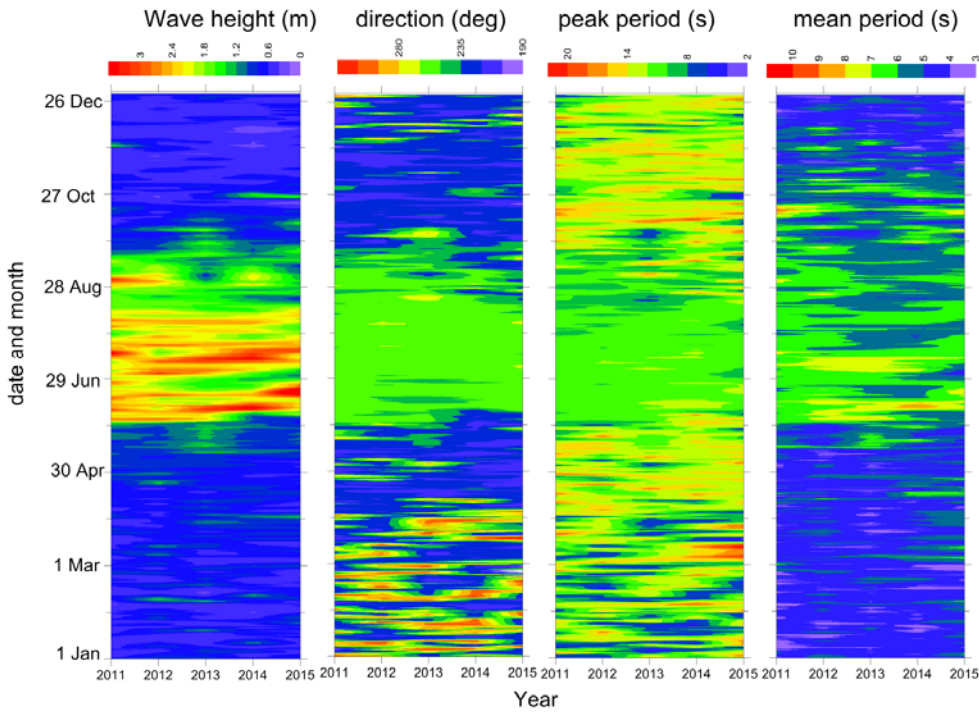


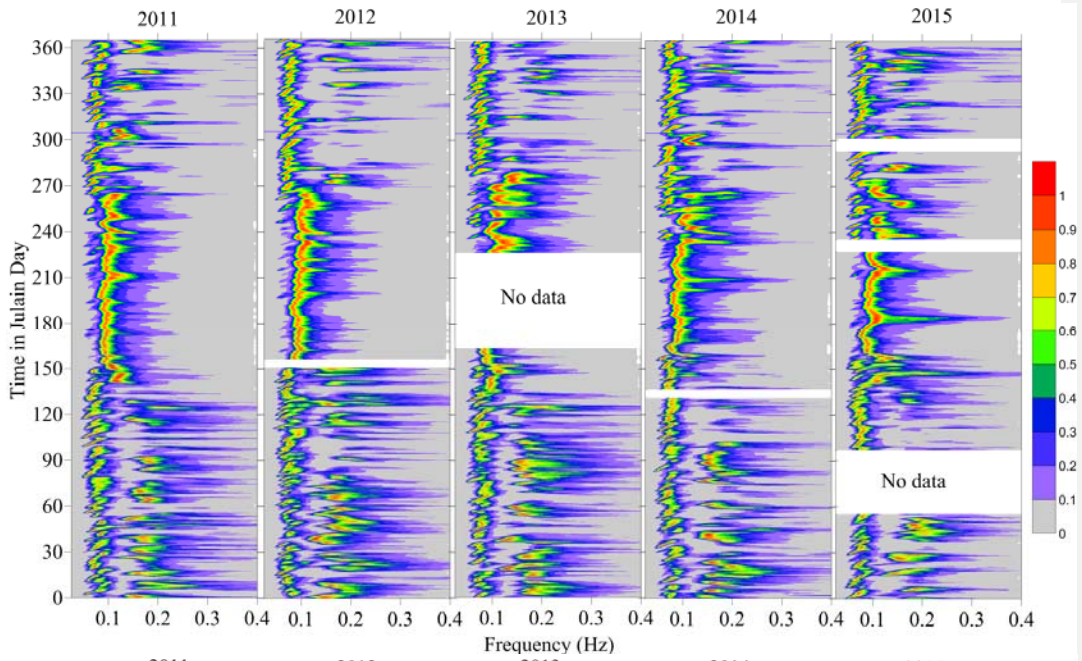
Figure 3. Wave roses during 2011-2015 (a) significant wave height and mean wave direction, (b) peak wave period and mean wave direction, (c) percentage of swell, (d) percentage of wind-sea and mean wave direction

711
712

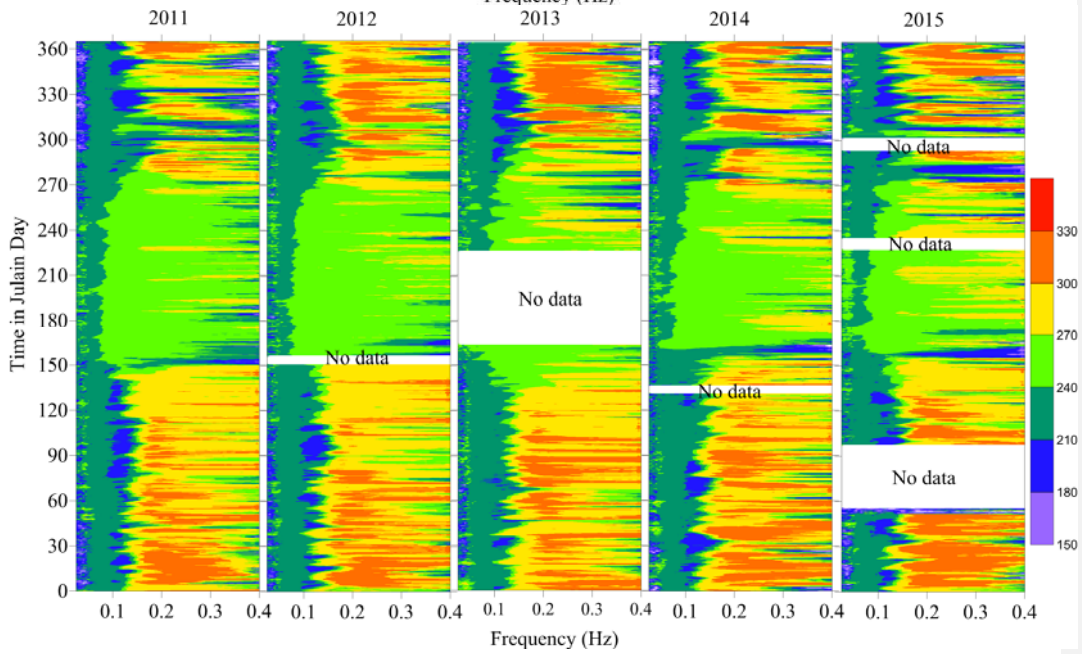


713
714 Figure 4. Date versus year plots of a) significant wave height b) mean wave direction, c) peak wave
715 period and d) mean wave period.
716

717
718



719



720
721 Figure 5. Temporal variation of normalized spectral energy density (top panel) and mean wave
722 direction (bottom panel) with frequency in different years

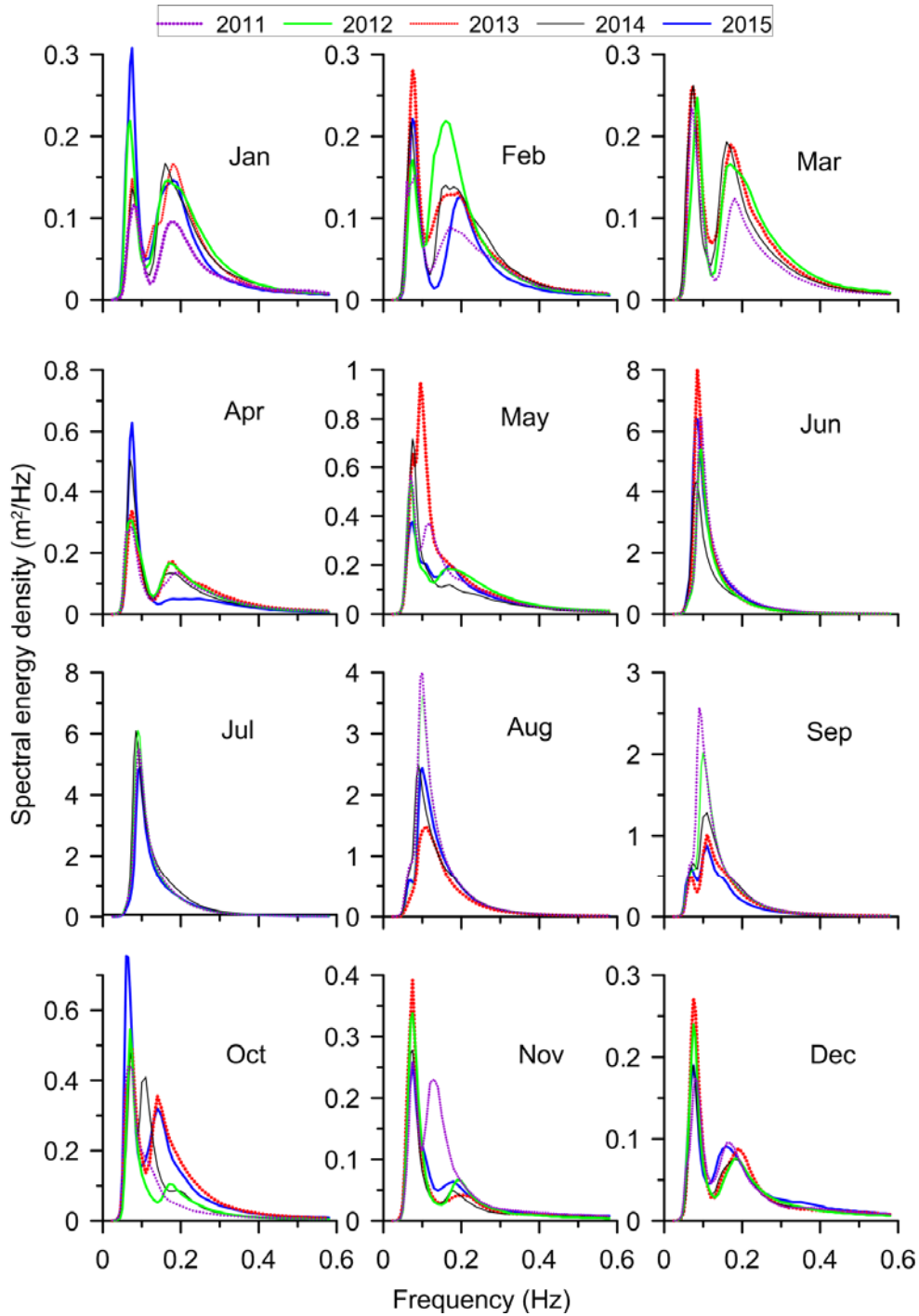
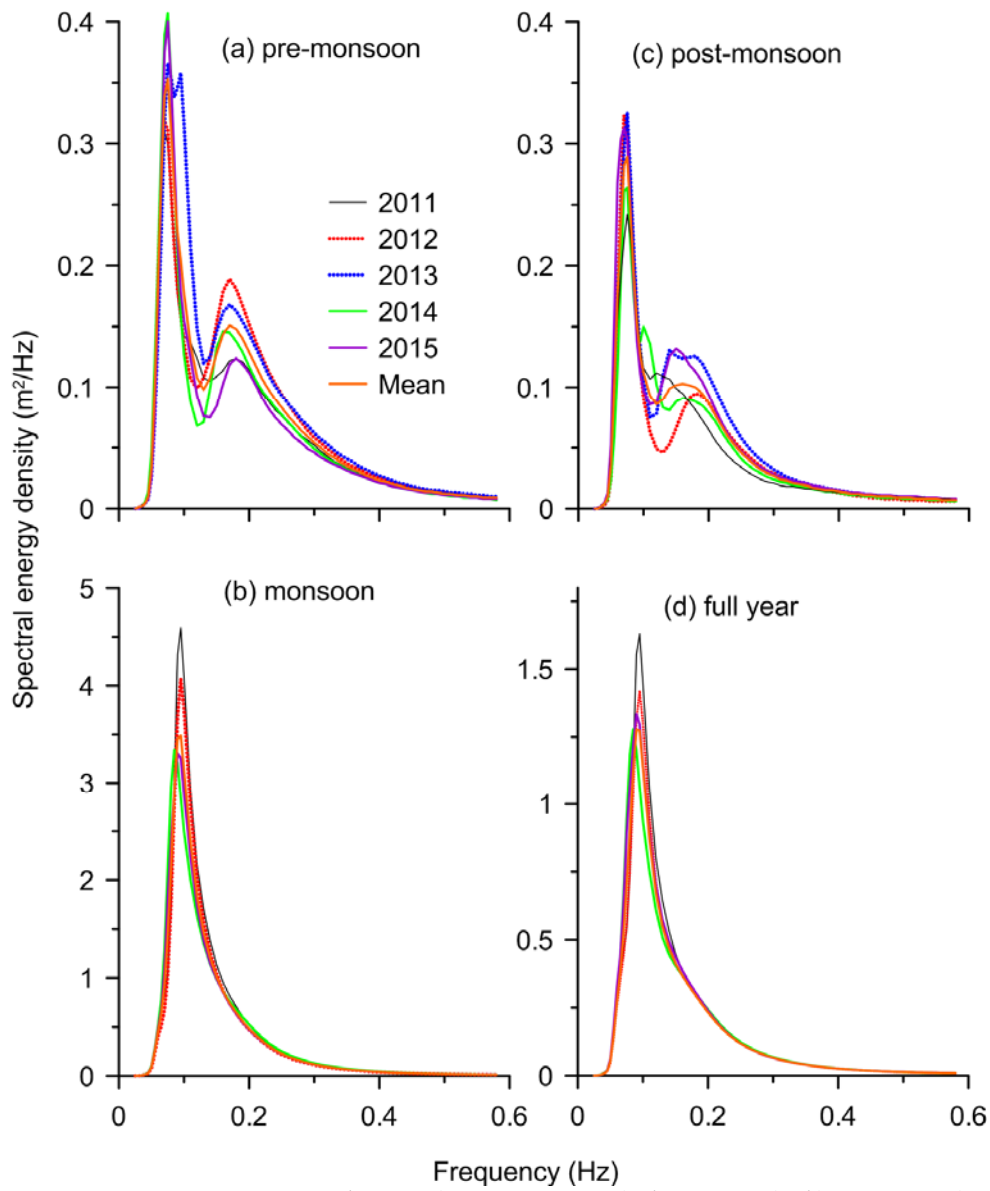
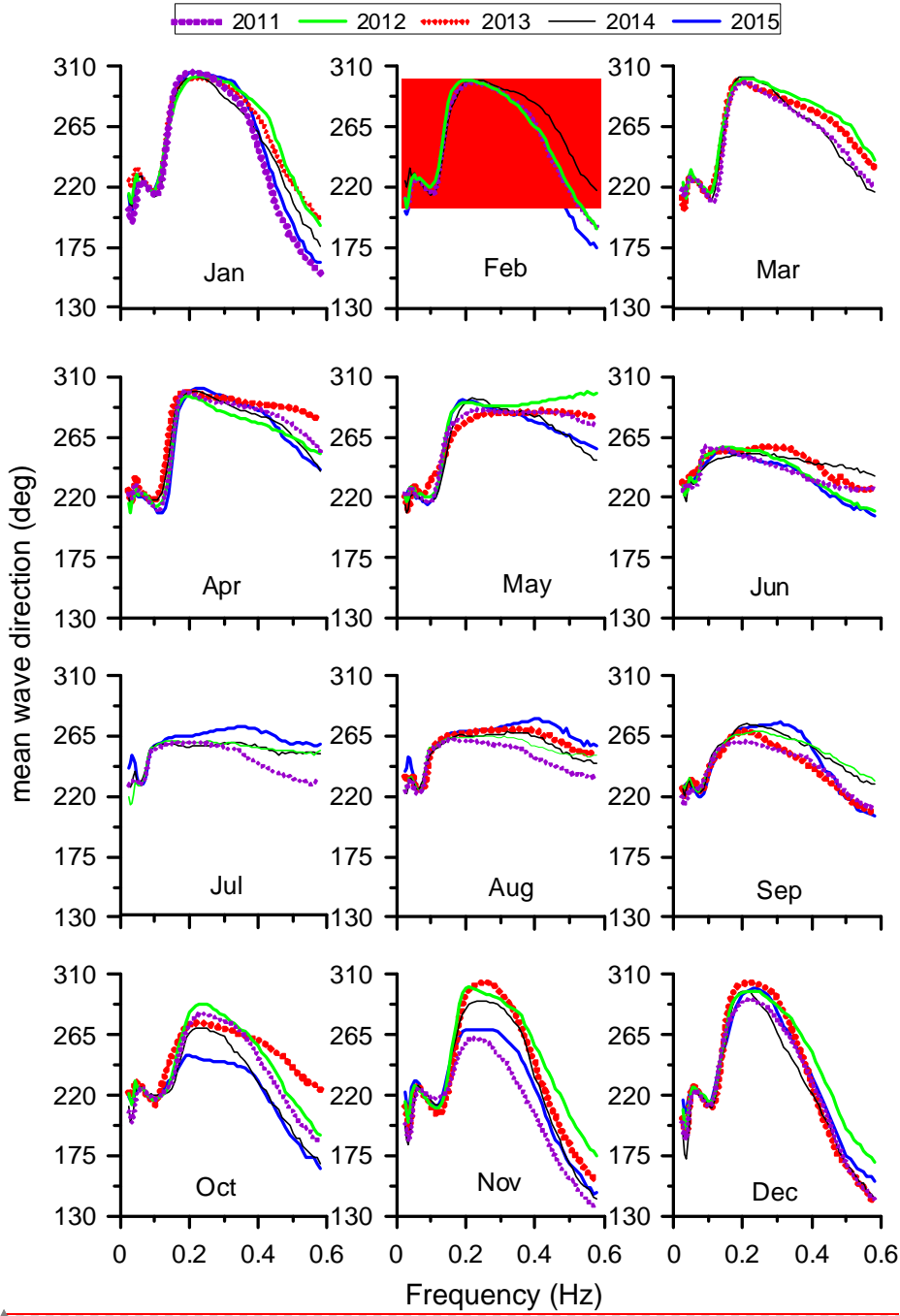


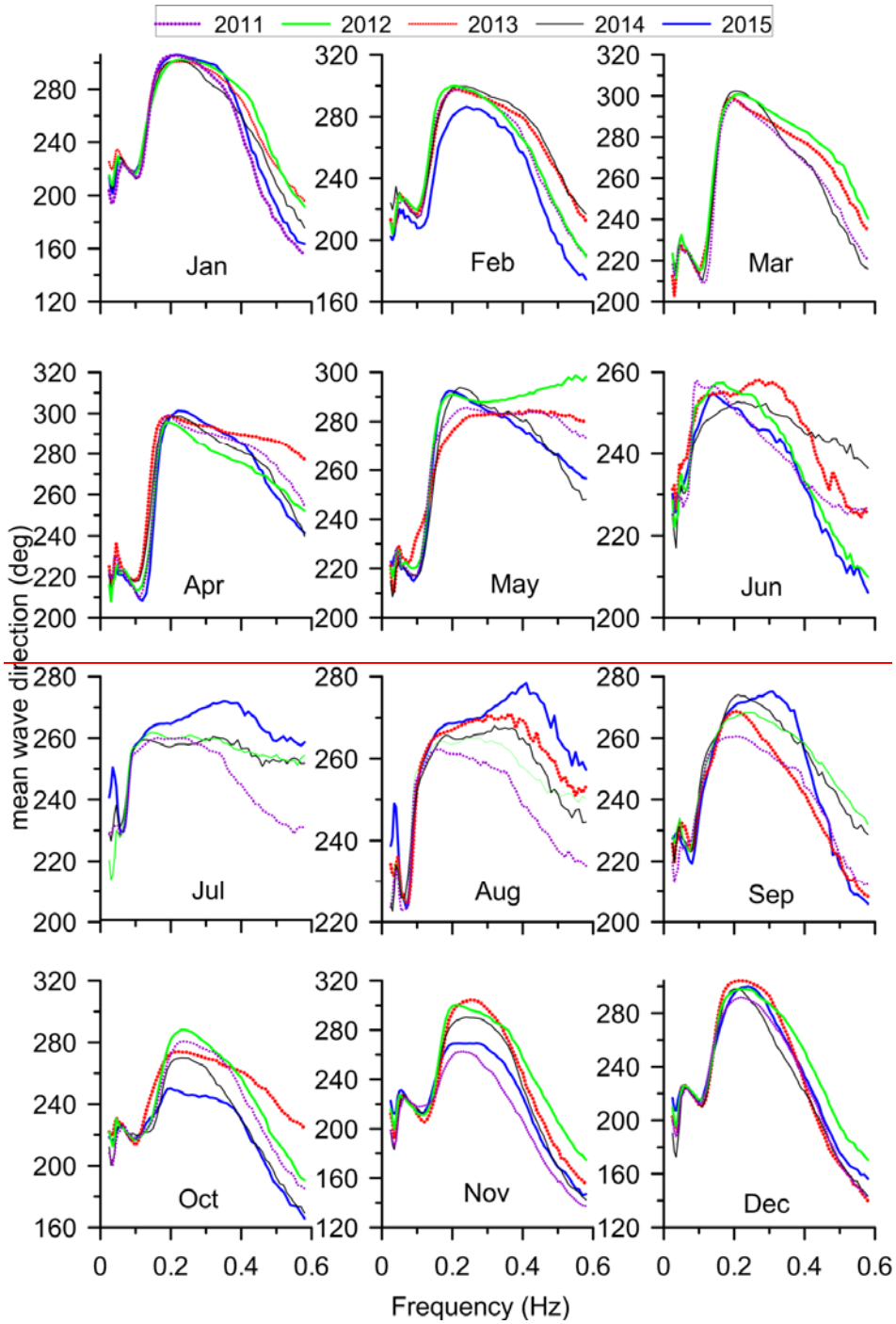
Figure 6. Monthly average wave spectra in 2011 to 2015



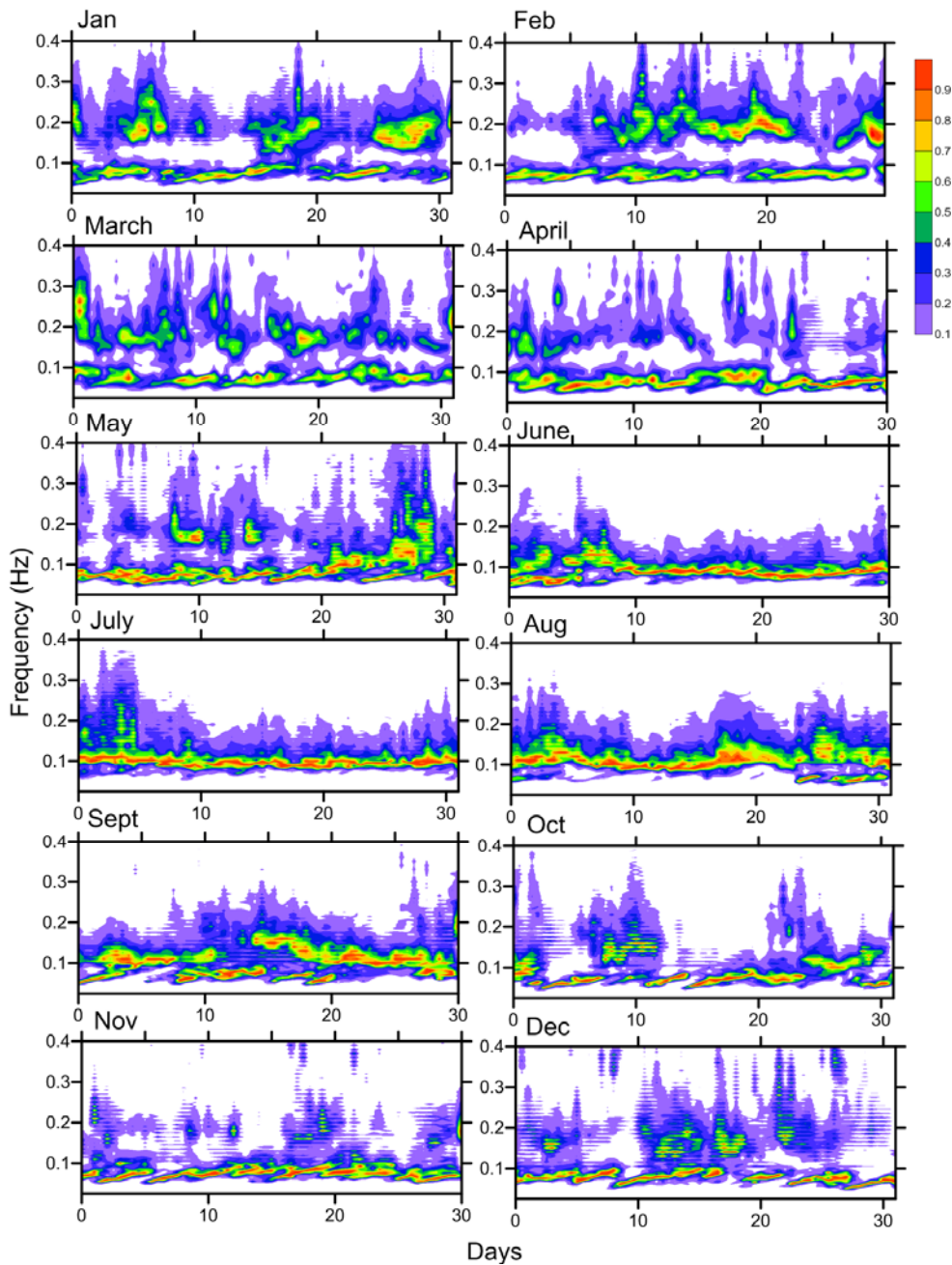
726
 727 Figure 7. Wave spectra averaged over a) pre-monsoon (February-May), b) monsoon (June-
 728 September), c) post-monsoon (October-January) and d) full year in different years

Field Code Changed

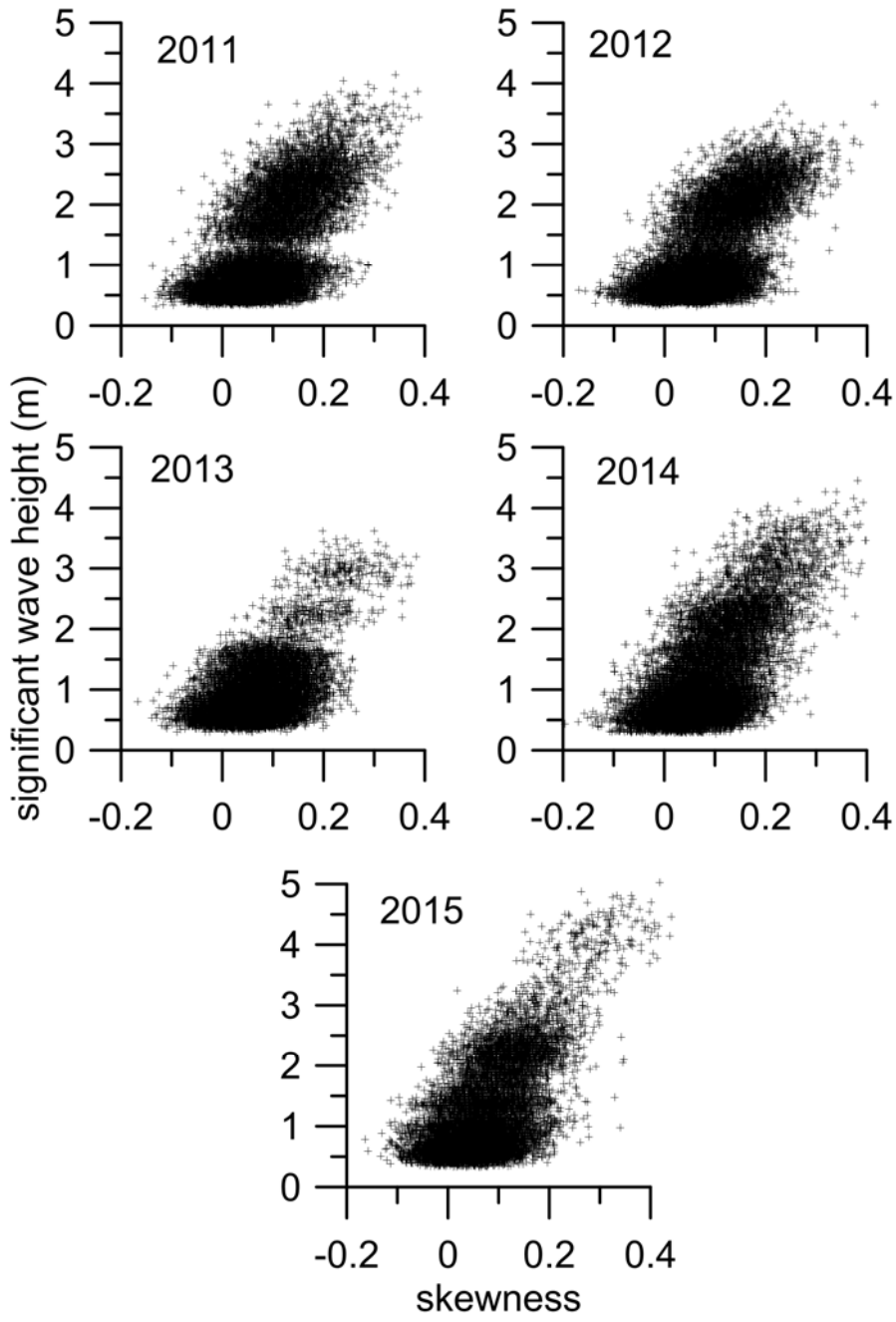




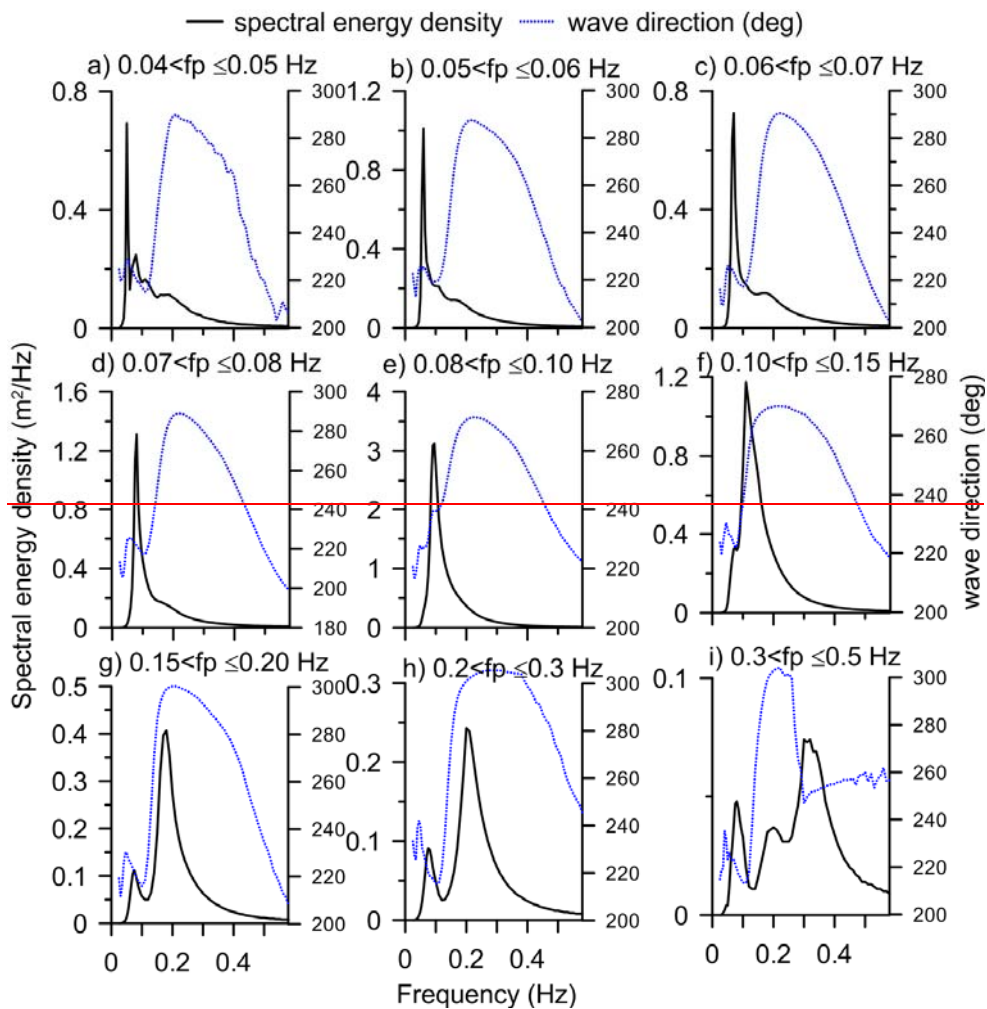
731
732 Figure 8. Monthly average wave direction at different frequencies in different months



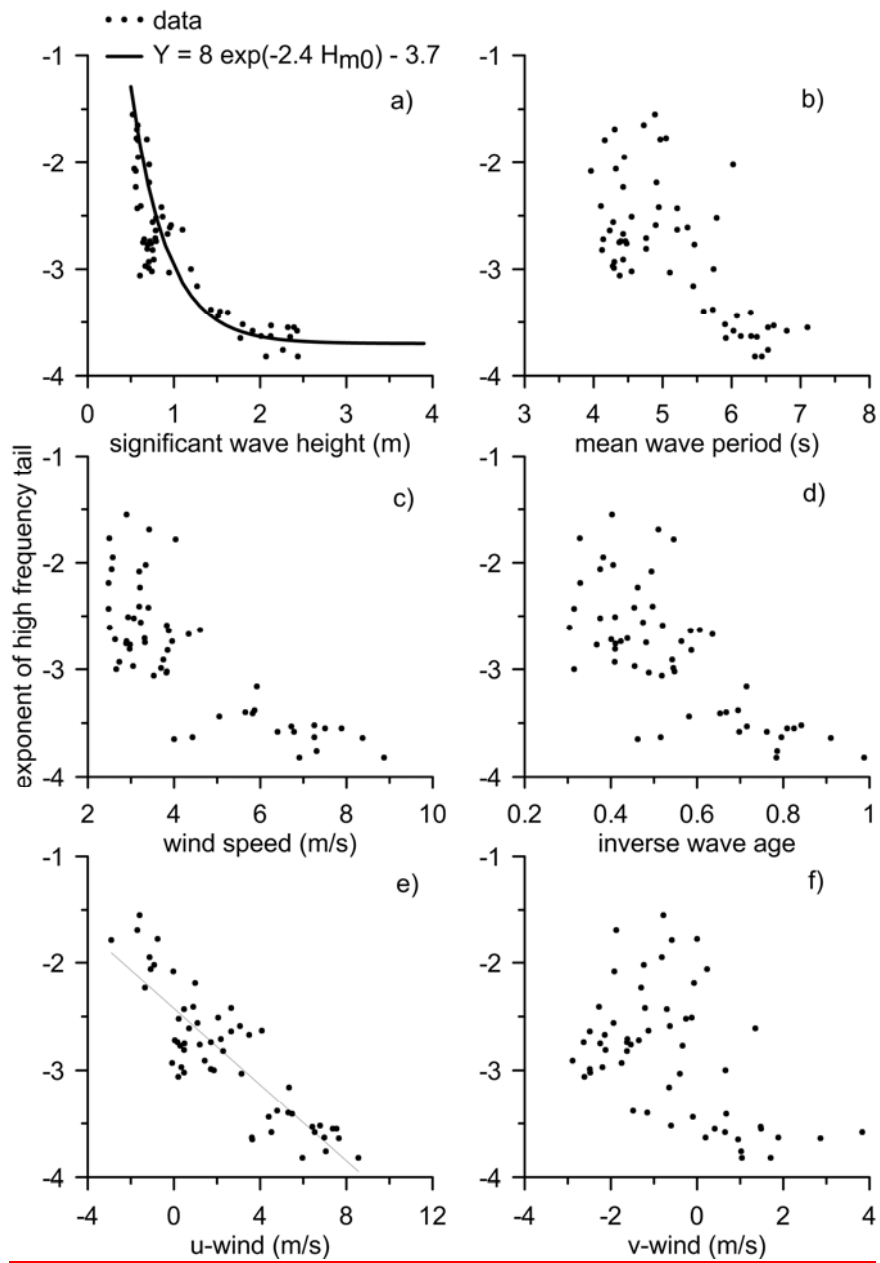
734
 735 Figure 9. Temporal variation of normalized spectral energy density in different months (data from
 736 2011 to 2015 used)
 737 |

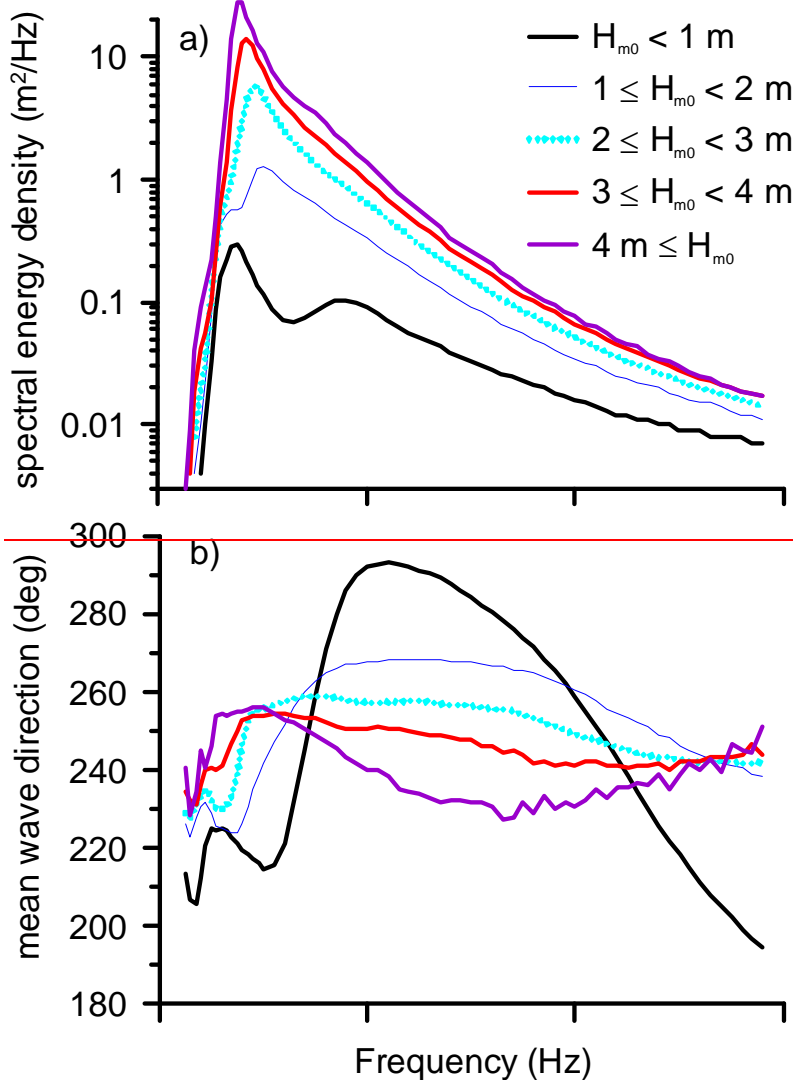


738
739



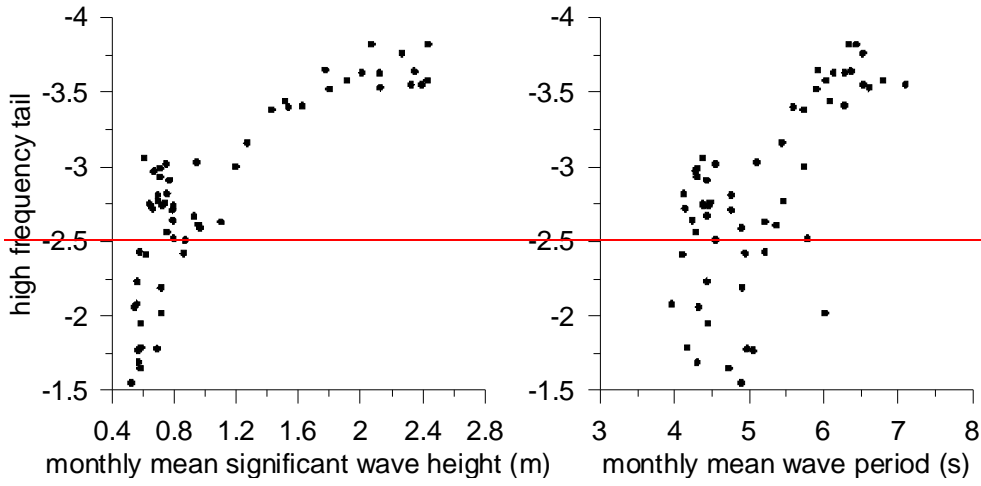
740 Figure 10. Scatter plot of significant average spectral energy density and average mean wave
 741 height with skewness direction of the sea surface elevation in waves grouped under different
 742 yearspeak frequency bins





745
746
747
748

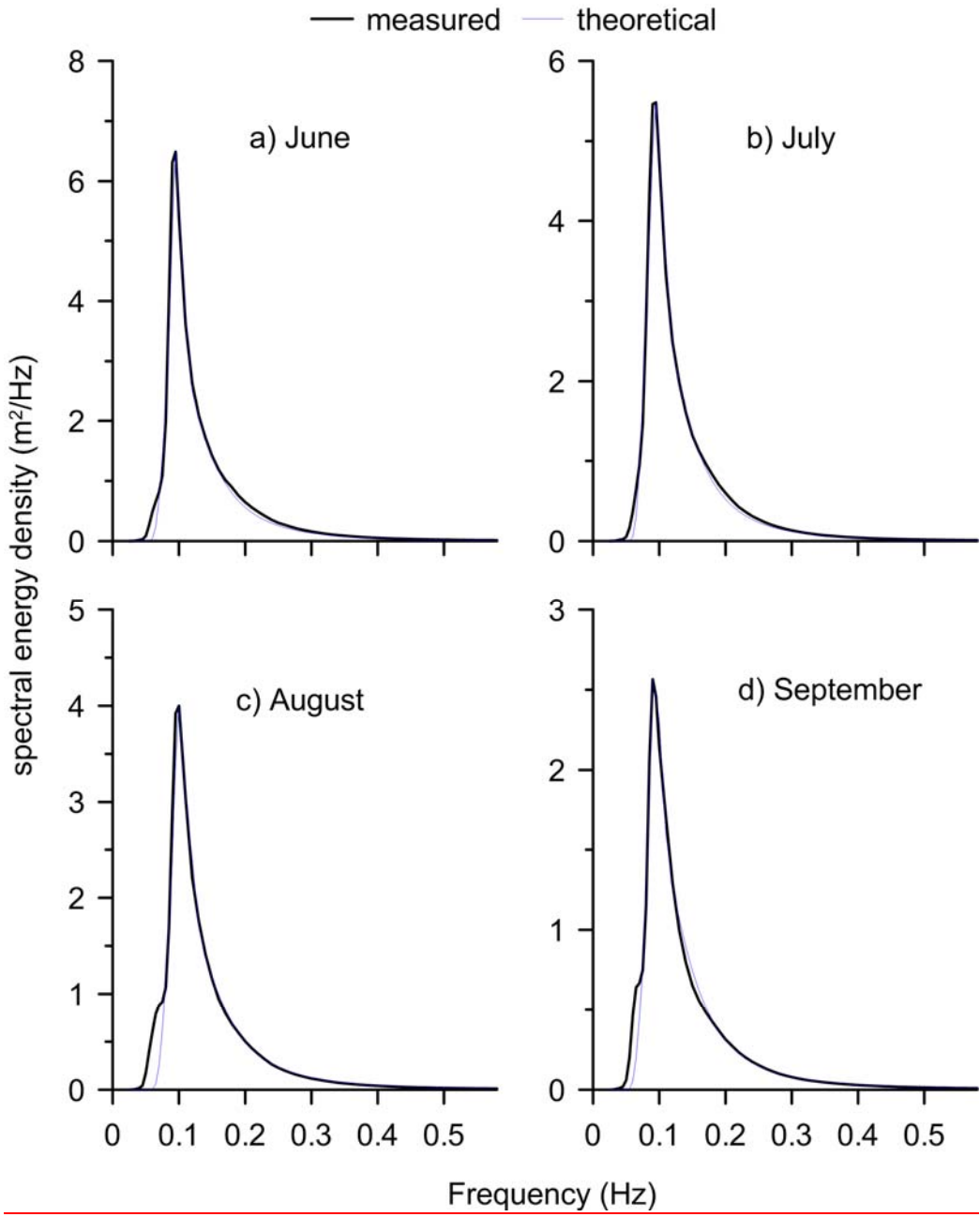
Figure 11. Plot of ~~exponent of the high-~~ average spectral energy density and b) average mean wave direction of waves under different H_{m0} with frequency

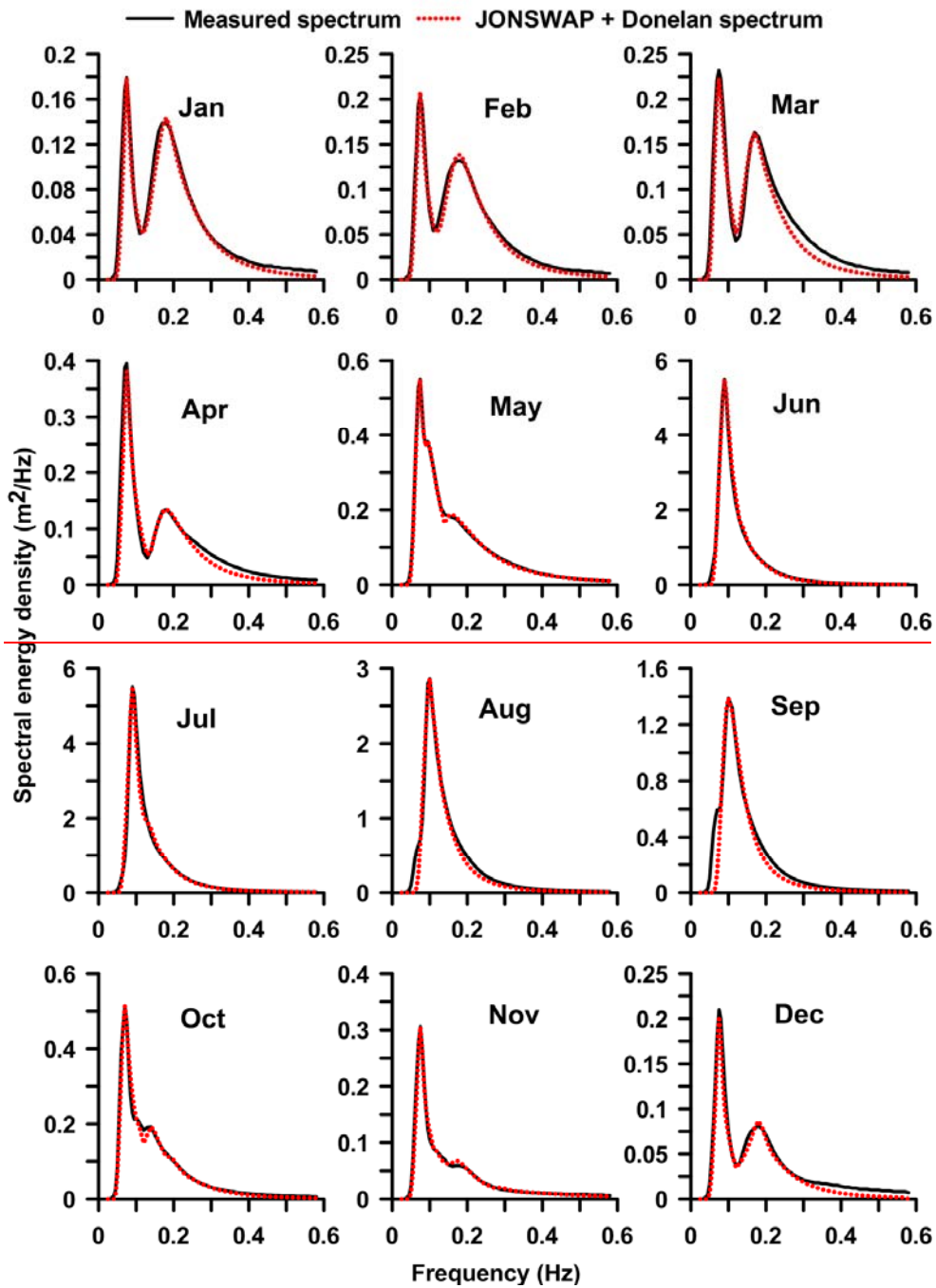


749
750
751
752

Figure 12. Plot of high-frequency tail with a) significant wave height b) (left panel) and with mean wave period, c) wind speed, d) inverse wave age, e) u-wind and f) v-wind (right panel)

Formatted: Left





754
 755 Figure 12. 13. Fitted theoretical spectra along with the monthly average wave spectra for a) June, b)
 756 July, c) August and d) September different month